DOKUZ EYLÜL UNIVERSITY
GRADUATE SCHOOL OF NATURAL AND APPLIED SCIENCES

PRODUCTION, CHARACTERIZATION AND DEVELOPMENT OF MULTIFUNCTIONAL COATINGS BY PHYSICAL VAPOR DEPOSITION FOR ULTRAVIOLET PROTECTION AND INFRARED STEALTH APPLICATIONS

by
Uğur KARTAL

March, 2021
İZMİR

PRODUCTION, CHARACTERIZATION AND DEVELOPMENT OF MULTIFUNCTIONAL COATINGS BY PHYSICAL VAPOR DEPOSITION FOR ULTRAVIOLET PROTECTION AND INFRARED STEALTH APPLICATIONS

A Thesis Submitted to the
Graduate School of Natural and Applied Sciences of Dokuz Eylül University
In Partial Fulfillment of the Requirements for the Degree of Master of Science in Metallurgical and Materials Engineering

by
Uğur KARTAL

March, 2021
İZMİR

M.Sc. THESIS EXAMINATION RESULT FORM

We have read the thesis entitled **"PRODUCTION, CHARACTERIZATION AND DEVELOPMENT OF MULTIFUNCTIONAL COATINGS BY PHYSICAL VAPOR DEPOSITION FOR ULTRAVIOLET PROTECTION AND INFRARED STEALTH APPLICATIONS"** completed by **UĞUR KARTAL** under supervision of **ASSOC. PROF. DR. METİN YURDDAŞKAL** and we certify that in our opinion it is fully adequate, in scope and in quality, as a thesis for the degree of Master of Science.

....

Assoc. Prof. Dr. Metin YURDDAŞKAL

Supervisor

....

Prof. Dr. Osman ÇULHA

Jury Member

....

Assist. Prof. Dr. Serdar YILDIRIM

Jury Member

Prof. Dr. Özgür ÖZÇELİK

Director

Graduate School of Natural and Applied Sciences

ACKNOWLEDGEMENT

I would like to thank everyone for their sincere support on this stressful but enjoyable journey that I have embarked on to obtain my master's degree.

Firstly, I would like to tell my interior appreciation to my advisor, Assoc. Prof. Dr. Metin YURDDAŞKAL, for his constructive ideas, supervision, support, understanding, contributions, and encouragement during my thesis.

I would also like to thank my committee members, Prof. Dr. Osman ÇULHA and Assist. Prof. Dr. Serdar YILDIRIM for reviewing my thesis and offering precious suggestions and sharing their visions.

I would like to present my special thanks to Dokuz Eylül University Electronic Materials Production and Application Center and its staff for the resources they enable for me. Also, I would like to thank Assoc. Prof. Dr. Mustafa EROL, Assoc. Prof. Dr. Tuncay DİKİCİ, Eyyüp Can DOLUEL, and Begüm UZUNBAYIR for their precious help, support, and nice friendship.

Finally, and most importantly, my family's support and belief in me has always motivated me. My mother Göksel KARTAL and my father Hasan KARTAL deserve the greatest thanks for their love and support, as they are always by my side. I should also thank my brothers Umut KARTAL and Yasin KARTAL for their endless support to me. Also, I would like to thank Burcu ÇALMA who never lost her faith in me and always supported me with love.

Uğur KARTAL

PRODUCTION, CHARACTERIZATION AND DEVELOPMENT OF MULTIFUNCTIONAL COATINGS BY PHYSICAL VAPOR DEPOSITION FOR ULTRAVIOLET PROTECTION AND INFRARED STEALTH APPLICATIONS

ABSTRACT

People are exposed to intense sunlight during the day. UV-A and UV-B rays that can reach the world from ultraviolet rays can be quite harmful for human health. Both people and objects can emit infrared wavelengths that produce thermal emissions that can be detected with a thermal camera. Therefore, recently highly infrared reflective materials have been of interest, for example in achieving infrared stealth. Within the scope of this thesis, infrared and ultraviolet reflective coatings with titanium dioxide / copper-aluminum / titanium dioxide sandwich structure on polyester fabric were manufactured using magnetron sputtering technique. Coated fabric samples were examined with the aid of X-ray diffractometer, scanning electron microscope, X-ray photoelectron spectroscopy, UV/VIS/NIR spectrophotometry, FTIR spectroscopy and thermal camera. The results showed that the sandwich thin film on the polyester fabric reflects ultraviolet and infrared wavelengths. The applicability of the protective coatings produced within the scope of the thesis on polyester textile products we use in daily life has been proven. Thus, the body can be protected from the harmful ultraviolet rays of the sun, the contact of infrared rays with the skin is prevented and a heat barrier can be created by preventing the spread of infrared rays from the body. Thus, a new generation of multi-functional fabrics was produced for use in both the health sector and the defense industry.

Keywords: Magnetron sputtering, ultraviolet, infrared, thin film

ULTRAVİYOLE KORUMA VE KIZILÖTESİ GİZLİLİK UYGULAMALARI İÇİN FİZİKSEL BUHAR BİRİKTİRME YOLUYLA ÇOK FONKSİYONLU KAPLAMALARIN ÜRETİMİ, KARAKTERİZASYONU VE GELİŞTİRİLMESİ

ÖZ

Gün içerisinde insanlar yoğun güneş ışınlarına maruz kalmaktadır. Morötesi ışınlarından dünyaya ulaşabilen UV-A ve UV-B olarak adlandırılan ışınlar insan sağlığı açısından oldukça zararlı olabilmektedir. Hem insanlar hem de nesneler, bir termal kamera ile tespit edilebilen termal emisyonlar üreten kızılötesi dalga boyları yayabilir. Bu nedenle, son zamanlarda, örneğin kızılötesi gizliliğinin elde edilmesinde, yüksek oranda kızılötesi yansıtıcı malzemeler ilgi konusu olmuştur. Bu tez kapsamında, polyester kumaş üzerine titanyum dioksit / bakır-alüminyum / titanyum dioksit sandviç yapılı olan kızılötesi ve morötesi yansıtıcı kaplamalar magnetron saçtırma tekniği kullanılarak üretildi. Kaplanmış kumaş numuneleri X-ışını difraktometresi, taramalı elektron mikroskobu, X-ışını fotoelektron spektroskopisi, UV/VIS/NIR spektrofotometrisi, FTIR spektroskopisi ve termal kamera yardımı ile incelendi. Sonuçlar, polyester kumaş üzerindeki sandviç yapılı ince filmin morötesi ve kızılötesi dalga boyunu yansıtıcı özellikte olduğunu gösterdi. Tez kapsamında üretilen koruyucu kaplamaların günlük hayatta kullanmakta olduğumuz polyester tekstil ürünler üzerine uygulanabilirliği ispatlandı. Böylece vücudun güneşin zararlı morötesi ışınlarından korunması, kızılötesi ışınların cilt ile temasının engellenmesi ve kızılötesi ışınların vücuttan yayılması engellenerek ısı bariyeri oluşturulması sağlanabilir. Böylece hem sağlık sektöründe hem de savunma sanayinde kullanılmak üzere çok işlevli yeni nesil kumaş üretimi gerçekleştirildi.

Anahtar kelimeler: Magnetron saçtırma, morötesi, kızılötesi, ince film

CONTENS

LIST OF FIGURES

Page

LIST OF TABLES

Page

CHAPTER ONE
INTRODUCTION

1.1 Background

In recent years, there has been considerable academic attention made on visible transparent, near infrared (NIR) and ultraviolet (UV) reflective thin films (Mavrić et al., 2018; Miao et al., 2015; Miao et al., 2014). Transparent conductive oxides (TCOs) are one of the potential candidates for UV and NIR reflective films due to their high visible transparency and high concentration of free electrons (Kumarakuru et al., 2014; Okuhara et al., 2011; Shi et al., 2013).

Since IR detection will be prevented by IR reflective coatings, it has a wide application area in military equipment and vehicles and is of great importance in this field (Kim et al., 2016). Ultraviolet protection films, sometimes referred to as UV protective agents, are among the most important studies applied to textile materials in order to protect people and textile materials from the harmful effects of UV radiation (Khan et al., 2018). UV light has the potential to initiate chemical reactions that can harm human health and textile fibers due to its more energy than visible light (Kocić et al., 2019). However, films need to be heat treated or warmed at the time of application in order to show the best UV and NIR reflection. This limits the functional applications of TCO films. In this context, TCO/metal/TCO multilayer films have attracted high attention as a highly promising way, thanks to their performance without heat treatment.

With the development of nanotechnology, various engineering studies have been done extensively to functionalize textile materials (Liu et al., 2007). It has limited the functionalization applications of traditional textiles due to its disadvantages.

To solve these problems, magnetron sputter deposition has proven to be one of the most promising technologies for producing nanostructured textile materials due to the advantages of low processing temperature (Deng et al., 2008), stability in quality, high deposition rate, multifunctionality (Jiang et al., 2011; Yip et al., 2009), and higher bond strength between coating and substrate (Wei et al., 2008).

1.2 Organization of the Thesis

In this thesis, TiO_2/Cu-Al/TiO_2 material with a TCO/metal/TCO sandwich composite structure was coated on a polyester textile product as a thin film by the physical vapor deposition method. The main purpose of the thesis is the optimization of the thin film production and to determine the effect of film thickness on structural, morphological, and optical properties of UV and NIR reflective thin films.

Chapter 1 presents an introduction to the thesis with a short explanation of thin films. Also, here the organization of the thesis has presented.

In Chapter 2, the theoretical background of light-matter interaction, electromagnetic spectrum, and thin films are explained. Detailed information about thin films such as production methods, applications, and materials are given in this chapter.

Chapter 3 consists of a literature review part about sandwich sequenced heterogeneous structured thin films.

The experimental part of the thesis was presented in Chapter 4. The synthesis and characterization methods of the desired thin films were given in detail. Names, properties, and information about the used chemicals at the production steps were listed. The presentation of the characterization instruments used in thesis studies is at the end of Chapter 4. Structural, morphological, chemical, and optical properties were characterized via X-Ray Diffractometer (XRD), Scanning Electron Microscope (SEM), X-ray photoelectron spectroscopy (XPS), UV Spectrophotometer (UV/VIS/NIR), Fourier transform infrared spectroscopy (FTIR) and thermal camera.

In Chapter 5, the general results of characterization were given and interpreted. The implications for the causes of these results were scientifically discussed in detail. In order to make a better analysis, some results were written on graphics and interpreted.

Finally, overall conclusions of the study and future plans are presented in Chapter 6.

CHAPTER TWO
THEORETICAL BACKGROUND

2.1 Light-Matter Interaction

The “color” of a material is a function of the interaction between light and an object. If the material absorbs light of certain wavelengths, these colors are not visible in the reflected light, only the reflected wavelengths reach our eyes; this makes the object appear in a specific color. For example, leaves appear green because chlorophyll, a pigment, reflects green by absorbing the blue and red colors of the spectrum (Fig. 2.1).

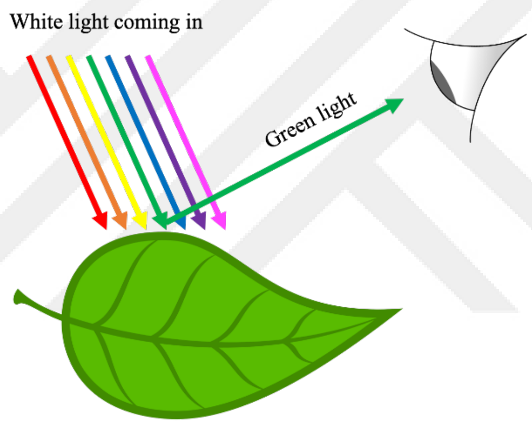

Figure 2.1 Illustration of a leaf reflecting incoming light as green

Generally, light (I) coming on the material is transmitted (T), absorbed (A), or reflected (R) by the material (Eq. 1). This phenomenon was shown in Figure 2.2. When the material is reduced in size, the scattering (S) of light affects its color or transparency.

$$I = T + A + R \tag{2.1}$$

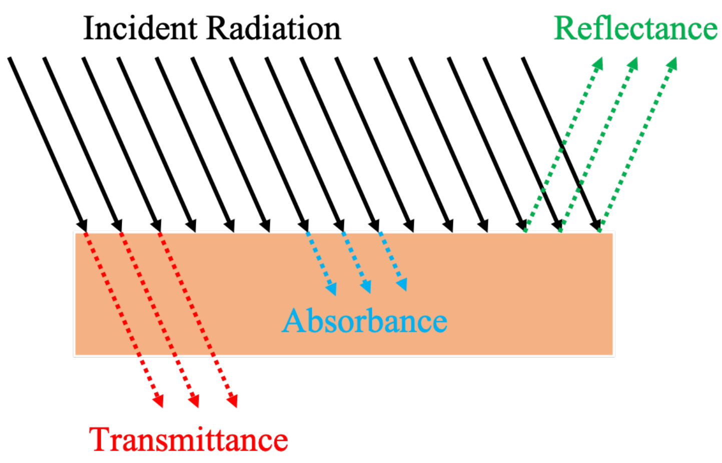

Figure 2.2 Different basic behaviors of light during material interaction

The return of light hitting a flat surface to the original environment is called *reflectance*. In this case, the incident wave and the reflected wave are on the same plane.

Absorbance is a process related to energy transformation. The energy levels of the substance determine the wavelengths of the absorbed light. Absorption is a molecular phenomenon, based on the chemical identity and structure of the substance, and is related to electronic transitions, vibrations, rotations. Some frequencies in the beam passing through layers such as transparent solid, liquid, or gas are kept selectively as a result of absorption. Here, electromagnetic energy is transferred to the atoms or molecules that make up the sample; The particles move from a low energy state to higher energy states or “excited states”. At room temperature, most substances are in the “ground state” where they have the lowest energy level. Absorption is related to the transition of particles from the ground state to the high energy states. Atoms, molecules or ions have a certain number of energy levels. In order for the light to be absorbed, the energy of the excitation photon must be equal to the energy difference between the ground state of the absorbing particles and any excited state.

The ability of light to pass through a material is called *transmission*. It has been experimentally observed that the propagation rate of the beam in a transparent material is lower than in a vacuum. The rate of advance also depends on the types and concentrations of the atoms, ions, or molecules in the environment. The interaction that causes the transmission can be explained by the change in the electric field of the beam. The changing electric field causes the bound electrons of the particles in the environment to fluctuate and make each particle polarized. Provided that the light is not absorbed, the particles hold the polarization energy for a very short time (10^{-14}-10^{-15} s) and extract it again without any change; the particles also return to their original state.

Scattering is a phenomenon comparable to the wavelength of the incident beam when the beam hits a surface; Therefore, it is a physical process that depends on the cluster size, the refractive index of the cluster, and the refractive index of the suspension medium (Fig. 2.3). Scattering is just a physical interaction and while energy transformation does not occur, it is directed in many directions. The wavelength of incoming and outgoing light is the same. Once the light hits the clusters in the colloid and is directed once, it can encounter another cluster and be redirected. Maximum scattering occurs for wavelengths twice the size of the cluster. As a ray passes through a substance, its ions, atoms, or molecules hold the energy of the beam for a very short time and become polarized; After a period of 10^{-14}-10^{-15} s, the particles release the energy they hold and return to their original state. The released ray is in all directions. If the particles are smaller than the wavelength of the beam, almost all of them disappear except the beam traveling in the original direction.

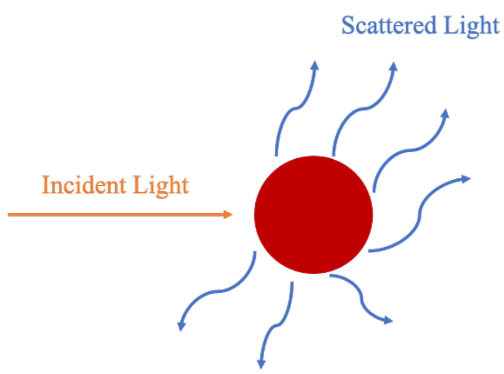

Figure 2.3 Scattering of light

Scattering caused by particles with wavelengths smaller than the wavelength of the beam is called *Rayleigh Scattering*. The intensity of scattering depends on the inverse of the fourth power of the wavelength of the beam, as well as the size of the particles and the ability to be polarized. Rayleigh scattering is elastic as the energies of the scattered photons do not change. The energy of the incident photon is too small to move the atom to an excited level.

In cases where the size of the particles in the environment is comparable to the wavelength of the beam, the scattering can be observed as the *Tyndall effect* or *turbidity*. Under the Tyndall effect, the longer wavelength is transmitted more, while the short wavelength is reflected more by scattering.

2.2 Electromagnetic Spectrum

In modern physics, light or electromagnetic wave is defined as two complementary forms, theoretically a wave in an electromagnetic field (Fig. 2.4) and another definition as a massless particle flow called photon (Güzel et al., 2015).

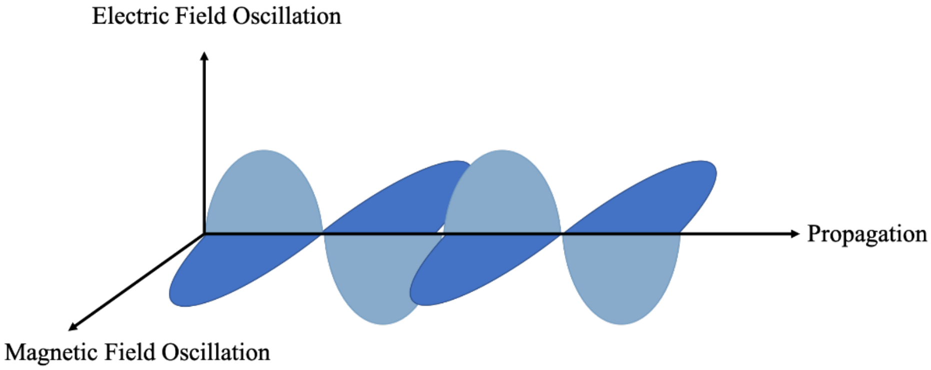

Figure 2.4 An electromagnetic wave is a pair of electric and magnetic fields that propagate in the direction indicated by the arrow and at the speed of light

Electromagnetic waves are a type of energy that spreads very rapidly in a vacuum. More and more physical events that we experience on a daily basis, such as the rising of sunlight, the microwave cooking our meals, and also activating the radios and televisions due to the electromagnetic field, are the situations that make us feel the presence of the electromagnetic wave. X-rays, ultraviolet rays, microwaves and radio waves can be counted among the main electromagnetic waves. Radio waves, TV waves, and microwaves are types of electromagnetic waves. They differ from each other only by their wavelengths. Waves in the electromagnetic spectrum range from very long radio waves to shorter gamma waves from the size of the nucleus of an atom. Electromagnetic waves propagate over a very large area according to their wavelength or energy. Electromagnetic spectrum regions can be shown as in Figure 2.5.

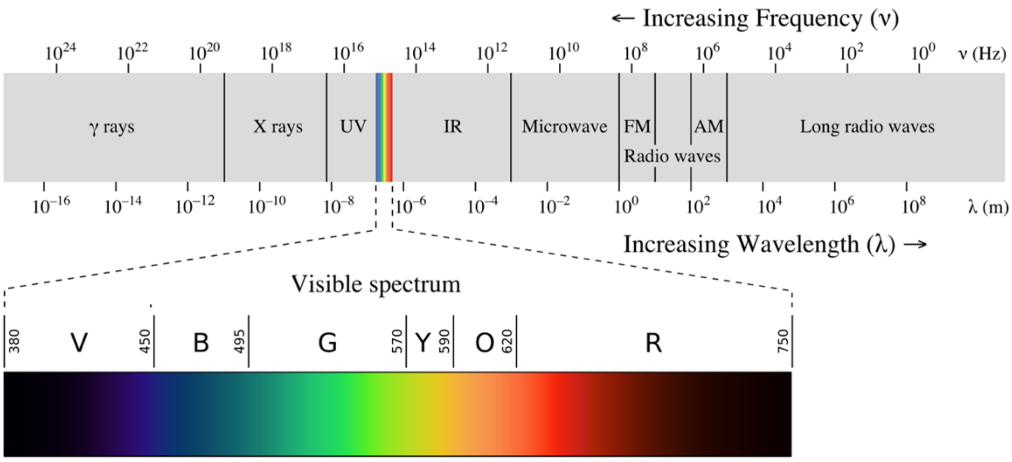

Figure 2.5 Electromagnetic Spectrum (Güzel et al., 2015)

2.2.1 UV and IR Irradiation

The region with a narrow radiation around 10^{-7} m of a wide electromagnetic spectrum defined by wavelength and frequency, especially with wavelengths between 100 nm and 400 nm, is called UV (Matts, 2006). The radiation in the 400 nm to 700 nm wavelength region in which the human visual phenomenon is activated generates "light" because the photoreactive cells of the human retina are only sensitive to this wavelength. It is therefore inappropriate to refer to "UV" as "light". The individual excitation quantum of electromagnetic radiation is known as the photon. Therefore, UV is a narrow waveband of electromagnetic radiation that acts as photons in waves. Waves are measured not only in wavelengths but also in frequency. Wavelength is measured in meters, while frequency is measured by the number of waves passing through a specific point in 1 s.

Simply put, the higher the frequency and energy, the shorter the wavelength of electromagnetic radiation. Regarding the UV region, this is a very important relationship. Because the higher the energy of a UV photon, the greater its reactivity with human biology. This results in splitting the UV waveband into three distinct spectral regions: UVC, UVB, and UVA (Coblentz et al., 1931).

Most modern dermatologists and photobiologists have redefined these three wavebands as follow:

- UVC: 200 nm to 290 nm
- UVB: 290 nm to 320 nm
- UVA: 320 nm to 400 nm

IR radiation is an electromagnetic energy and is located between visible light and microwave regions in the electromagnetic spectrum. This region defines electromagnetic radiation between 1.8 and 3.4 µm wavelengths (Fasina et al., 2001). Human body at normal temperature radiates around 10 µm (Ignatov, 2014). IR rays are divided into 3 within itself according to wavelength and emission temperature:

- Short wave or near IR region, 0.72-2µm
- Medium wave or middle IR region, 2-4 µm
- Long wave or far IR region, 4-1000 µm

However, the lower and upper boundaries of the wavelengths that define IR differ slightly in the literature, and there is no sharp distinction between these regions.

2.2.1.1 Beneficial Effects of UV and IR Rays on Human Body

The beneficial effects of human exposure to ultraviolet radiation are relatively low. It is best known that UVB radiation promotes the synthesis of vitamin D in the skin (Fig. 2.6) (Keane et al., 2018). People get very little natural vitamin D in food, but they mainly get it as pro-vitamin D. To maintain the synthesis of vitamin D from Pro-vitamin D and to prevent the body from running out of vitamin D, the body needs 10-15 minutes of sun exposure every day. Keeping children home and protecting their skin from UV exposure causes low vitamin D levels in their bodies during the winter months. Ultraviolet radiation is one of the methods available to manage persistent psoriasis, persistent eczema and other conditions. Additionally, it's possible that exposure to ultraviolet radiation may have psychological benefits. The well-known problem of seasonal affective disorder that causes depression in winter in Northern European countries is mainly related to the absence of visible light. More research is needed in this area for treatment with UV rays (Mackie, 2000).

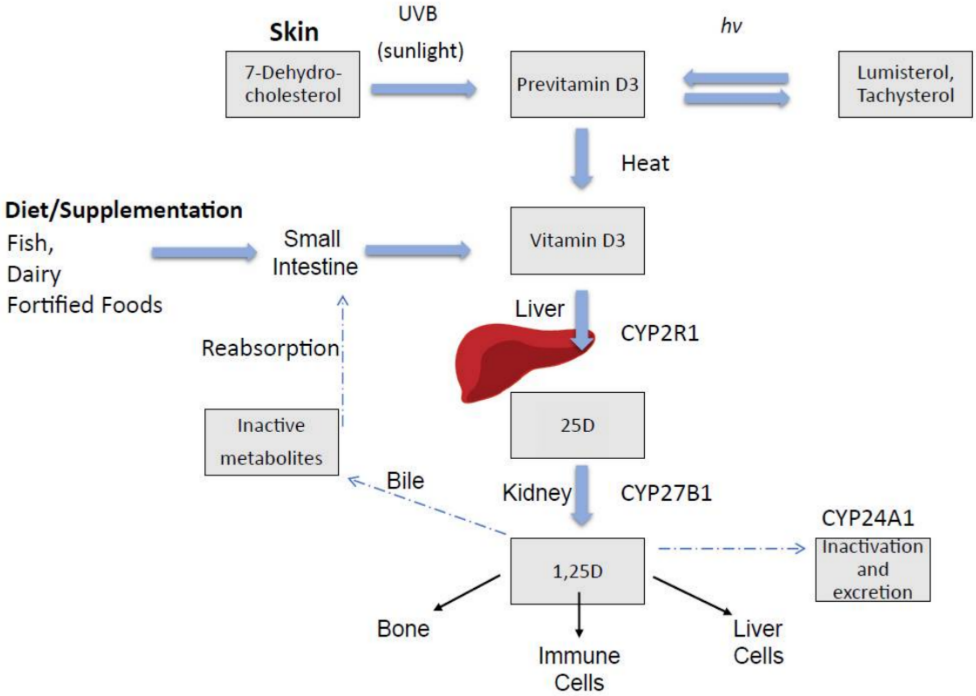

Figure 2.6 Vitamin D endogenous synthesis and metabolism (Keane et al., 2018)

It has been proven by various studies that far infrared waves have a positive effect on living organisms (Honda & Inoué, 1988; Hwang et al., 2014; Lin et al., 2013; Yuce, 2017). Far IR rays in the 4-14 μm wavelength range are considered beneficial for cell growth, and radiation at this wavelength is referred to by some as “rays of life” (Dyer, 2011).

The following health effects of IR therapy have been mentioned: It increases the amount of oxygen in the blood, rejuvenates muscle tissues and skin, provides tissue regeneration and rapid recovery, improves nervous system function, reduces lipids in skin tissue, improves metabolism, increases blood circulation, increases oxygen delivery and nourishment to soft tissue, helps to remove accumulated toxins, relaxes muscles and improves sleep quality (Lou & Lin, 2011).

2.2.1.2 Harmful Effects of UV and IR Rays on Human Body

Potential harms of UV radiation in humans are its effects on the skin, immune system and eyes. The dangers of excessive UV radiation on the skin can be caused by exposure to natural UV radiation in the form of sunlight or artificial sources. Skin deformation caused by excessive exposure is most prominent in people with white skin, pale skin, tanning and frequent burning. Chronic overexposure to ultraviolet radiation leads to a photoaging that is easily distinguishable from chronological or biological aging of the face, forearm, or back of the hand. Skin with this condition is usually thinner, wrinkled, and exhibits distinct pigmentation with mottling. Excessive dryness of the skin is also characteristic of photo aging (Cho et al., 2009; Pandel et al., 2013).

Another effect of UV radiation on human health is seen when the ability to repair genetically determined DNA is faulty after exposure. This is unplanned erroneous DNA synthesis (Mackie, 2000).

The skin is designed to protect the organism from injury and to act as a physical barrier against the external environment. However, while performing this task, the skin is exposed to IR radiation. Although depending on the dose, IR radiation may create free radicals in the skin, leading to situations that may cause therapeutic or pathological effects. IR radiation, reaching deeper than UV, penetrates the epidermal and dermal layers of the skin; as a result, it can damage the skin a lot (Fernández et al., 2016).

2.3 Thin Films

The fact that thin films of noble metals were used as decoration on glass and ceramics centuries ago, has increased the interest in thin film technology since the 1940s. Thin films, which form the basis of the micro and nanostructured optoelectronic materials industry and have an important place in technological and scientific research, are one of the most studied current research topics. Thin films are materials that are formed as a thin layer by arranging the atoms or molecules of the material to be coated using different production techniques on a substrate that helps the formation of the film, and the thickness is generally less than 1 μm (Sönmezoğlu et al., 2012). Nanocrystalline materials in thin film format allow the materials and tools made with these materials to increase their basic characteristics such as optical, mechanical and electrical characteristics at tremendous rates. In such materials, a gradual transition from solid to molecular structure is observed due to the increase in the number of particles forming the material. In addition, since the nanocrystal size of a thin film affects the band structure of the material, the fact that the particles forming the material are small enough causes the charge carriers to be in the quantum boundary and the band structures to dissociate into discrete energy levels (Pejova & Grozdanov, 2006). Thin film technology, which is one of the basic and determining elements of technological developments today, is found in most electronic devices, from personal computers and hardware used by humanity to communication systems. Thin films serving different purposes are used in different technological applications considering their various properties. Thin films have a very important place among the devices we use in almost every field in our daily life. Thin films are used in semiconductor / superconductor devices (Nomura et al., 2004; Simon et al., 1988), insulation and conduction coatings (Ge & Zhai, 2018; Kawazoe et al., 1997), circuit element construction (Erokhin & Fontana, 2011), reflective and non-reflective coatings (Ulbrich et al., 2013; Xu et al., 2013), interference filters (Goossens & Van Hoof, 2020), memory discs (Tverjanovich et al., 2020), protection against oxidation or corrosion (Khamseh et al., 2021), and sensors (Thai et al., 2020). The rapid change in thin film materials and equipment today; It creates new opportunities for the development of new processes, materials and technologies.

Therefore, many experiments and model systems have been developed to improve the previously known properties of basic physical and chemical properties related to thin film performance and structure in various applications and to increase the progress in this field. The combined results of experimental and theoretical investigations are a prerequisite for the development of new thin film systems and for shaping their structure and performance (Khan et al., 2020). Thin film production is an inexpensive method compared to the material to be integrated, because it is a method that can be easily deposited according to the substrate material to be coated, not the large and wide samples to be produced. Thin films must have suitable thickness, informatics and characteristics in order to perform the expected functions. Therefore, different production methods and production of better-quality thin films are carried out by trying to produce on different backing materials.

2.3.1 Applications of Thin Films

2.3.1.1 Optical Thin Films

Optical coatings are used in both reflective and refractive systems. In the 19th century, large-area (reflective) mirrors produced by spraying metallic silver (Park et al., 2015) or aluminum on glass were produced and put into use (Fig. 2.7). Aberrations typically occur in the refractive lens of cameras and microscopes, so they exhibit non-ideal refractive behavior. Previously, large sets of lenses had to be lined up along the optical path. However, today, optical lenses are coated with transparent multi-layer titanium dioxide (TiO_2), silicon nitride (Si_3N_4) or silicon dioxide (SiO_2) etc (Badri & Gilarlue, 2020; Du et al., 2021). coatings to solve these problems. Lenses only a few mm wide in smartphone cameras are a well-known example of the advancement in thin-film technology and optical systems. Anti-reflective coatings on glasses or solar panels are other examples of optical coatings (Zambrano et al., 2021).

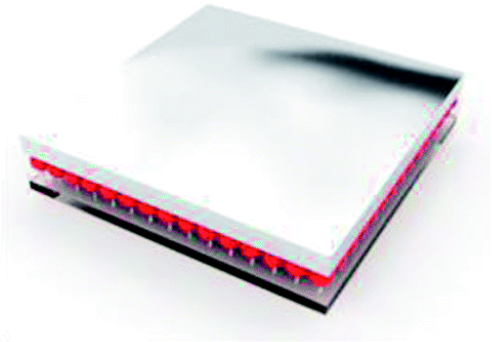

Figure 2.7 Silver film growth on a thiol-modified electrode (Park et al., 2015)

Another important type of optical coating is *dielectric coating*. These are formed from thin layers of material such as magnesium fluoride (MgF_2), calcium fluoride (CaF_2) and various metal oxides deposited on the optical base. By changing the coating material, thickness and number of layers, it is possible to change the reflectivity and transparency of the coating in a fairly wide range. The reflection coefficients of the surfaces can be lowered below 0.2% by forming an anti-reflective coating (AR), while it can also be increased above 99.99%. Thus, a highly reflective coating material (HR) is obtained. The level of reflection can also be adjusted to any specific value to produce a mirror that reflects a certain percentage of the light falling on it across some wavelengths and passes the rest. Such mirrors are often used in lasers and as beam splitter materials. Alternatively, the coating can be designed to act as an optical filter by reflecting light only in a narrow wavelength range.

2.3.1.2 Protective Thin Films

Protective thin films are generally applied to protect a workpiece from external influences. Protection can be provided to minimize contact with the external environment to reduce diffusion from the environment to the workpiece, or vice versa, to prevent diffusion from the interior to the outside. For example, anti-diffusion layers are often coated on the outside of the bottles to prevent out-diffusion of carbon dioxide (CO_2) discharged into acidic beverages contained in plastic bottles. As another example, it is coated with thin titanium nitride (TiN) films that separate electrically conductive aluminum lines from SiO_2 in the ground to prevent aluminum oxide

(Al_2O_3) formation. Generally, protective thin films are applied to prevent abrasion between mechanically moving workpieces.

2.3.1.3 Photovoltaic Thin Films

Thin film technologies are highly promising as a way to significantly reduce the cost of solar cells. The fact that thin film solar cells are cheaper to produce due to reduced material, energy, processing and capital costs is also effective. An example of the structure of the thin-film photovoltaic solar cells was shown in Figure 2.8 (Mohammad Bagher, 2015). Research on photovoltaic thin films is still ongoing and these products have limited commercial availability. It is generally classified as emerging or third generation photovoltaic cells. This class includes organic, dye sensitive and polymer solar cells (Arbab & Mola, 2019; Hamed & Mola, 2020; Patil et al., 2020). In addition to these, there are also quantum dot, copper zinc tin sulfide (CZTS), nanocrystal and perovskite solar cells (Hu et al., 2019; Lin et al., 2019; Liu et al., 2020; Yoo et al., 2019).

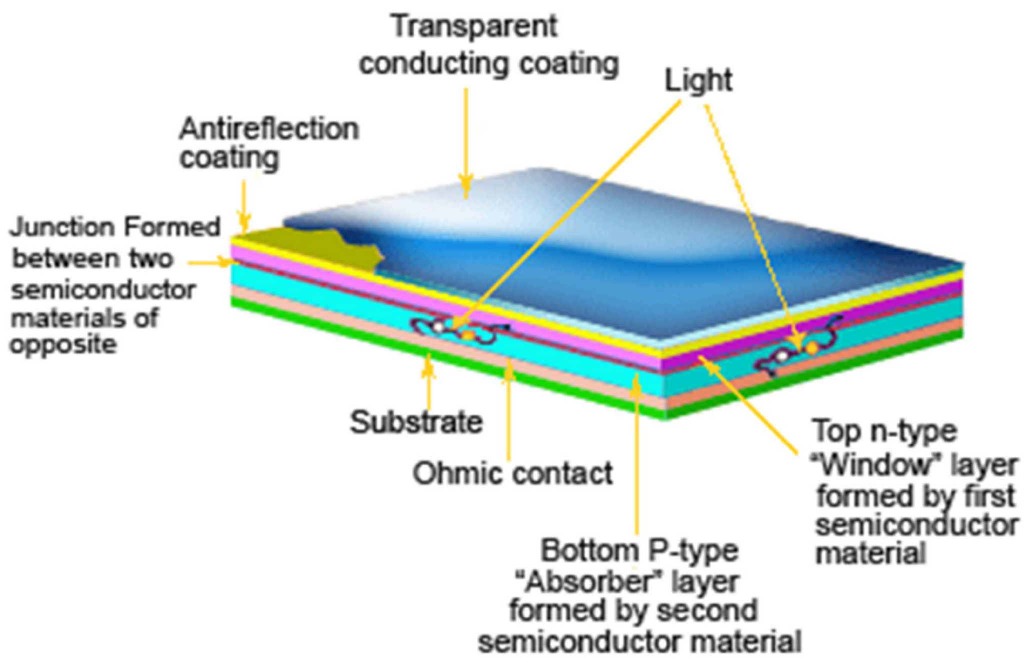

Figure 2.8 Structure of thin film solar cells (Mohammad Bagher, 2015)

2.3.1.4 Decorative Thin Films

Probably the oldest thin film applications are those used for decorative coatings. More than 5000 years ago in ancient India, thin 100 nm gold leaves were already used for decorative coatings. Although this kind of work was generally regarded as an art craft rather than an engineering or scientific discipline, it did not change the fact that thin films were used at that time. Today, thin film materials with variable thickness and high refractive index, such as TiO_2, are frequently applied for decorative coatings on glass that cause a rainbow-colored appearance. Transparency/opacity of decorative thin films can be controlled by changing the parameters of the thin-film production process (da Silva Oliveira et al., 2018) as shown in Figure 2.9. In addition, surfaces with a gold appearance can be prepared more cheaply by spraying TiN (Guo et al., 2019).

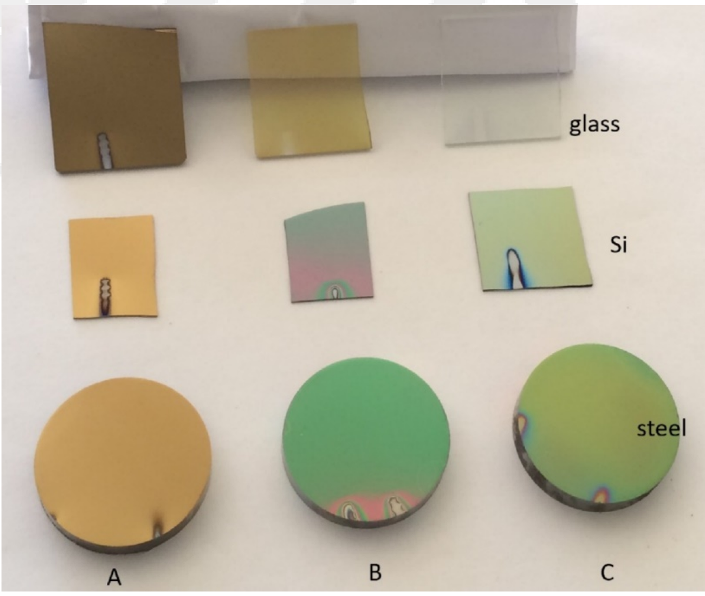

Figure 2.9 Zirconium oxynitride films deposited on three different substrates (da Silva Oliveira et al., 2018)

2.3.1.5 Electrically Thin Films

Thin films and alloys from basic metals such as copper (Cu), aluminum (Al), gold (Au) or silver (Ag) have been used in many applications in electrical equipment (Bobinger et al., 2017; Emami & Goodarzi, 2018; Lindner, 2020; Sarma, 2021). Due to their high electrical conductivity, they can carry electrical currents or applied voltages. Thin metal layers are used in many functional applications such as printed circuit boards, cables, sensors, transistors, capacitors, and various integrated circuits (Fukuda & Someya, 2017; Lee et al., 2014; Li et al., 2016; Syms et al., 2010). These layers can have varying thicknesses in the range of a few µm to several nm. Figure 2.10 shows a micrograph of a laterally configured TiN/Al:Cu/TiN metal stack in a microelectronic chip (Birkholz et al., 2010).

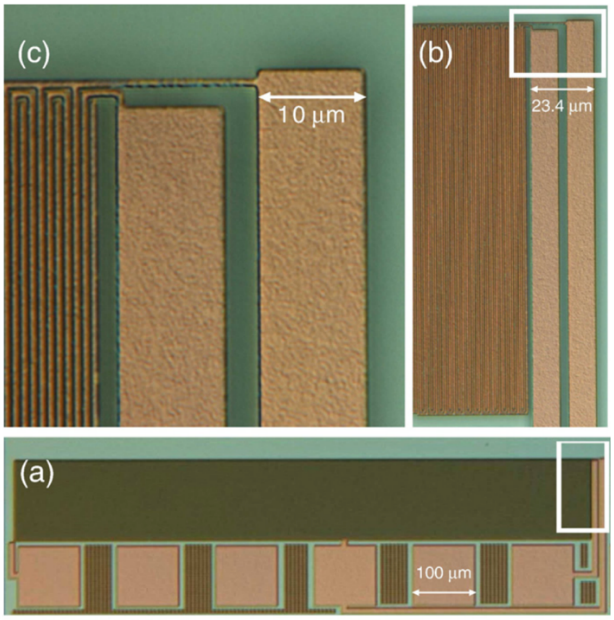

Figure 2.10 Optical micrographs of metallic meander structures of the TiN/Al:Cu/TiN multilayer stack. (c) and (b) are shown different magnifications giving the closed portions shown in (b) and (a), respectively (Birkholz et al., 2010)

2.3.2 Production of Thin Films

Thin films, which have an important place for scientific and industrial studies, were first used as decoration on glass and ceramics. Later, silver films were obtained on glass surfaces by using silver salts. The increase in scientific studies since the 19th century has brought along newer and more modern methods of obtaining thin films. The first thin film was obtained by "electrolysis" method in 1838, and later in 1852, Bunsen "chemical reaction" method, Faraday "evaporation in inert gas" method, Nahrwold and Kundt "Joule heating" method again obtained thin film (Savale, 2016).

However, these studies on thin films remained laboratory studies until the development of vacuum devices. After the vacuum devices were developed, the crystal structures, electrical and optical properties of thin films obtained by modern methods were started to be investigated. Basically, thin film production techniques are divided into various subgroups, as shown in Figure 2.11, according to the deposition techniques that allow the physical and chemical properties of the material surfaces to be changed, and the physical state of the material to be deposited.

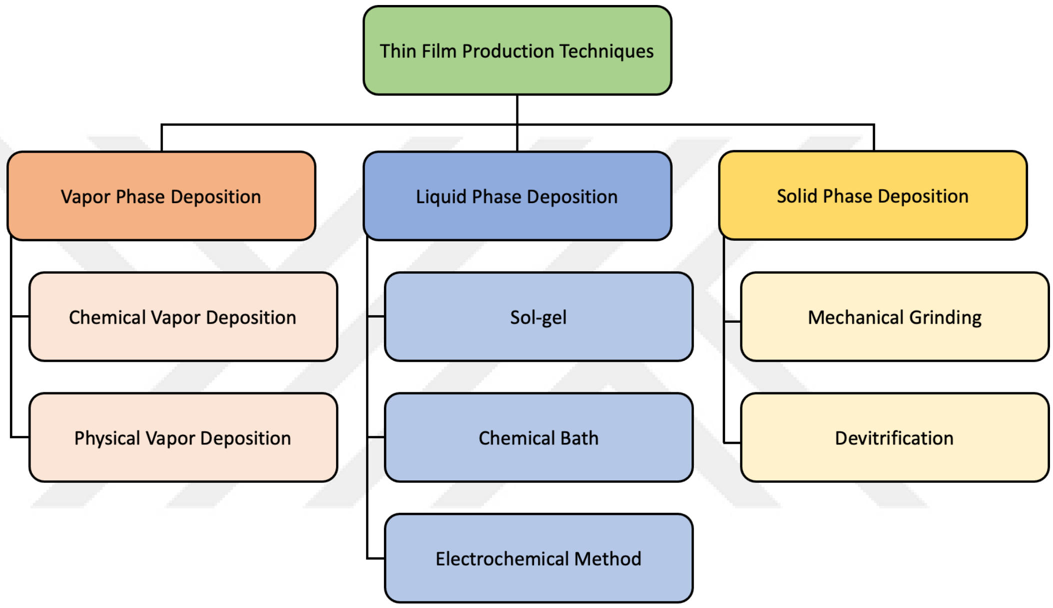

Figure 2.11 Thin film production methods

2.3.2.1 Vapor Phase Deposition

The vapor phase coating techniques, which enable to obtain high quality coatings without any restrictions on the coating or base material, are divided into two as chemical vapor deposition (CVD) and physical vapor deposition (PVD).

Although PVD coating technology has been known since the early 19th century, it has only found a place in the industry in recent years. The mechanism of this technique applied with different coating processes developed until today can be summarized as follows;

i) In a vacuum environment, the coating material evaporated by a heater is deposited as a thin film layer on the material to be coated,

ii) The solid state of the raw material is ionized with high energy and formed by reactive gases and then adhered to the material to be coated in a controlled manner.

At the end of the 19th century, especially with the increase of industrialization, abrasion resistance became a serious need and the first steps of the vacuum systems used today were taken in the 1960s. With the development of the semiconductor industry, the PVD technique, which has found a place in the industry, is used in many different fields such as micro-electronics, medicine, decorative purposes, applications requiring resistance to oxidation and corrosion (Lackner & Waldhauser, 2010; Lauwerens et al., 2001; Rossnagel, 1998).

The PVD coating method, which is based on the principle of removing the atoms from the surface by evaporating or sputtering solid or liquid materials in a vacuum environment and atomically or ionically depositing them on the surface of the substrate to be coated, is examined in two groups as "Evaporation" and "Sputtering". PVD techniques can be seen in Figure 2.12 (Rossnagel, 2003).

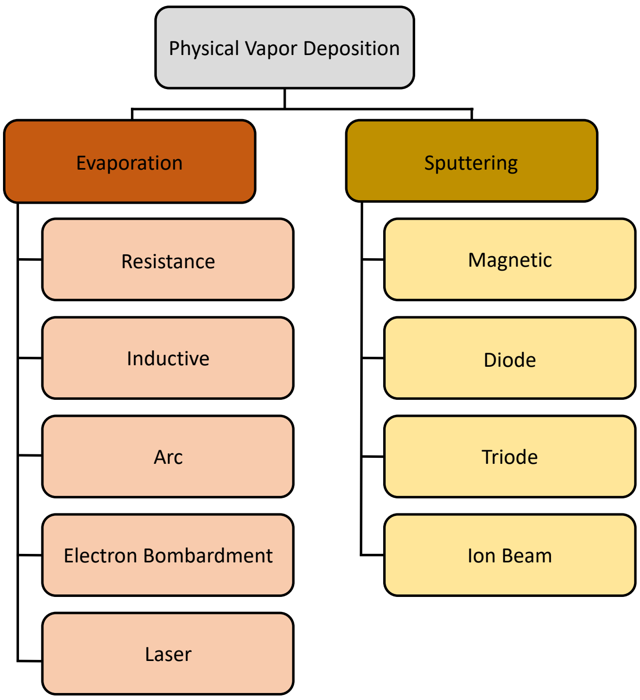

Figure 2.12 Physical vapor deposition techniques (Rossnagel, 2003)

The sputtering method is based on the principle of bombarding the surface of the target material with high-energy gas ions of accelerated atomic size, usually by means of a plasma or ion gun, sputtering the atoms from the surface and depositing the atoms detached from the surface of the target material into the vapor phase and deposited on the base material. Sputter coating was first observed by Grove in 1852 in a DC (direct current) gas glow discharge tube (Grove, 1852). The cathode material was deposited inside the tube by sputtering high energy ions from the cathode of the tube in the gas discharge. At that time, sputtering was undesirable as it caused the cathode to degrade. But today sputtering is widely used in surface cleaning, surface abrasion, thin film deposition and surface analysis (Harris et al., 2002; Ishizuka et al., 2000; Taglauer, 1990). The noble gas ions used in the sputtering method shown in Figure 2.13 hit the target material surface and give their energy to the material and thus sputter the atoms from the surface of the material.

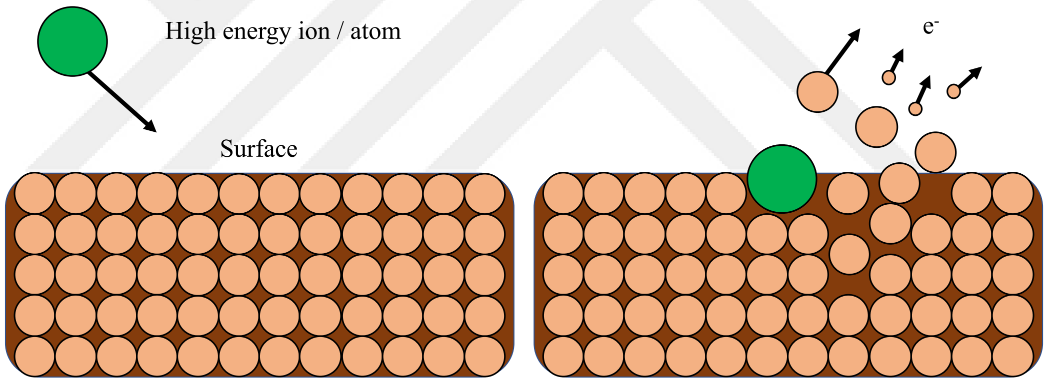

Figure 2.13 Mechanism of sputtering

Although many materials were successfully coated by the sputtering technique, the low deposition rate and ionization effect in the plasma and the increase in the substrate temperature limited the use of the system. Most of the advances in sputtering technology in recent years have been made in the magnetic field. This is because the magnetic field sputtering coatings are used in many industrial areas such as microelectronics, optics, turbine blades, magnetic and optical discs, and cutting tools (Budinovskii et al., 2019; Wei et al., 2002). The most important advantage of the sputtering method is that alloys with different evaporation rates at different vapor pressures can be successfully deposited without changing their composition. In addition, in this method, the possibility of macro particles to enter the film structure is very low. The adhesion of the resulting coatings to the substrate is very good and can be further improved by sputter cleaning the substrate. As a result, the quality and structure of the film obtained by sputtering is excellent. The disadvantages of the method are limited coating thickness and high cost because the electricity consumption in the sputtering method is much higher than in evaporation. PVD coatings obtained using the sputtering process are grouped as diode, triode, sputtering in magnetic field and sputtering with ion beam.

The *diode sputtering system* shown schematically in Figure 2.14 consists of a pair of planar electrodes, one of which is the anode and the other the cathode. There is a coating material on the upper surface of the cathode in contact with the plasma, and a water-cooled chamber under the cathode. The material to be coated is placed in the anode. After the sputter chamber is placed under vacuum, a glare discharge occurs when an inert gas such as argon gas is given to the chamber with a pressure of 13.3 Pa (10^{-1} torr) and a voltage of a few kilovolts and a resistance of 1-10 kΩ is applied between the electrodes. The positive ions in the glow discharge hit the cathode surface and sputter the coating material from there, forming a thin film on the surface to be coated (Nelis & Pallosi, 2006). If the coating material is conductive, DC is applied to create a glow discharge and this system is called *DC diode sputtering*. In case the coating material is insulating, radio frequency (RF) voltage is used instead of direct current voltage to create glow discharge. This system is called *RF diode sputtering* (Chiarello et al., 2017). Although the diode sputtering method is widely used due to its ease of use, it has many disadvantages such as not using secondary electrons, low deposition rate, overheating of the substrate due to bombardment of high energy particles, and very limited deposition surface area (Sönmezoğlu et al., 2012)

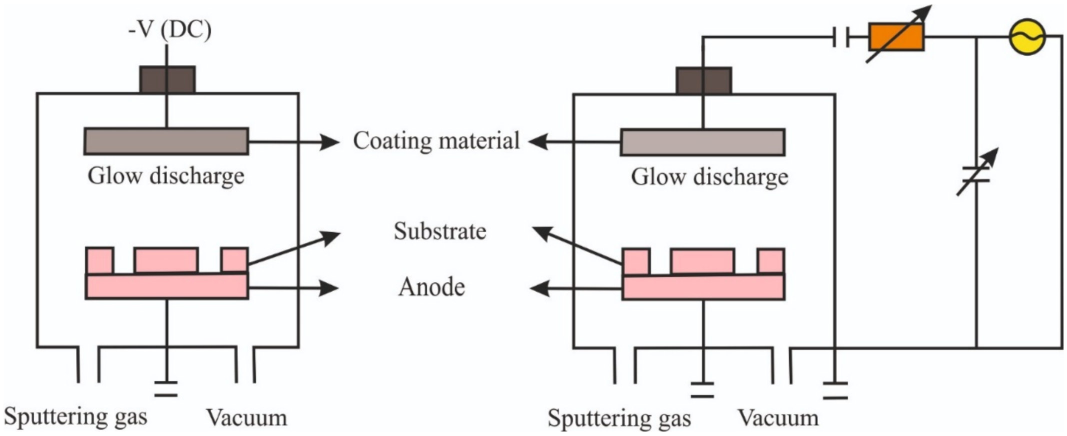

Figure 2.14 Diode sputtering system (a) DC (b) RF

In the *triode sputtering* system, there is a heater and a positive potential electrode in addition to the diode system to increase ionization at low pressures and maintain glow discharge. The heater and electrode increase the sputter efficiency by increasing the gas ionization degree. The primary anode placed opposite the cathode has a potential close to the gas ionization potential that causes plasma to form. Under these conditions, it offers the opportunity to obtain a homogeneous plasma even at low pressure values.

The most used triode system is the hot cathode triode system shown in Figure 2.15. The hot cathode emits electrons during thermionic emission and these electrons are thrown into the glow discharge system. In this case, the ionization efficiency increases. Thus, the glow discharge occurs by applying lower voltage (50-100 V) and at lower pressures (6.6-0.13 Pa). For this reason, the deposition rate with triode sputter method is higher (a few hundred nm/min) than the deposition rate by diode sputter method. The main disadvantage of the triode sputtering method is that the lifetime of the filaments is shortened in the presence of reactive gas (Sönmezoğlu et al., 2012).

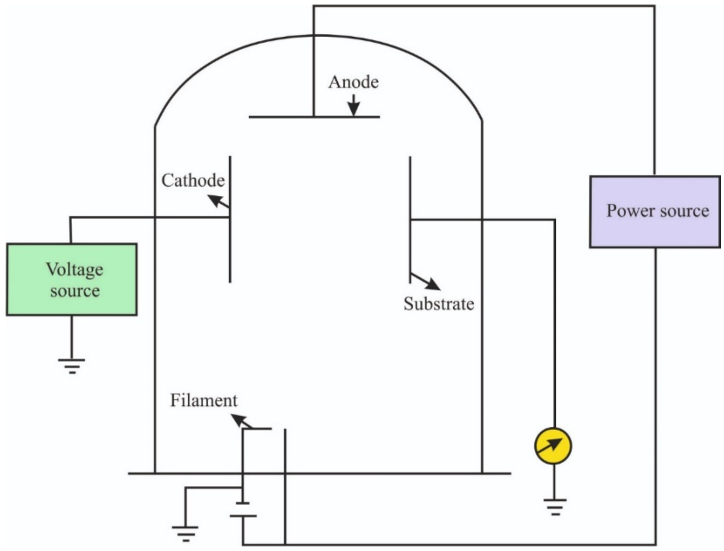

Figure 2.15 Triode sputtering system

Another sputtering method, the *ion beam sputtering* technique, provides the opportunity to work at high pressures. This technique is based on the principle of sputtering the target indirectly by bombarding it by a dependent ion source. Figure 2.16 shows the ion beam sputtering method schematically (Saraf et al., 1998).

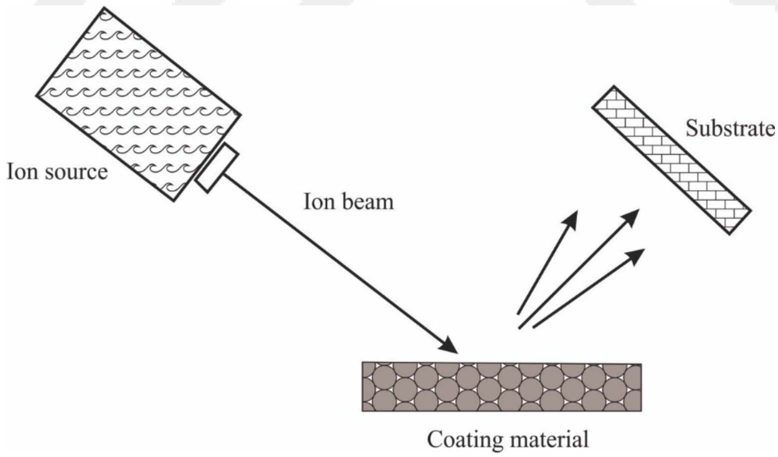

Figure 2.16 Sputtering with ion beam (Saraf et al., 1998)

The most used ion sources are "Kaufman source" and "Duoplasmatron". Duoplasma, where ions are created by providing arc discharge, is the oldest ion source used. In recent years, Kaufman ion source has been used. In the Kaufman ion source with hot filament cathode, ions are obtained by forming plasma (Kaufman & Robinson, 1982). The disadvantages of the ion beam sputtering method, which provides good adhesion at low temperatures, are the need to work at high gas pressures, the small diameter of the ion beam (~1 cm) and therefore the deposition rate is low. In addition, the same thickness of film cannot be formed on materials with large surface area (Sönmezoğlu et al., 2012).

In the *magnetic field sputtering* method, the target material is placed on a holder consisting of a water-cooled magnet or electromagnets. One pole of the magnet is placed in the central axis of the coating material and the second pole at the edges of the coating material. The arrangement of the magnets in this way ensures that the electric and magnetic fields are perpendicular to each other on the coating material. Electrons in the plasma move in the direction of ExB. In other words, the motion of electrons is perpendicular to both the electric field (E) and the magnetic field (B). As seen in Figure 2.17, the movement path of electrons in the direction of ExB is parallel to the surface of the coating material and forms a closed loop (Maurya et al., 2014). At the surface of the coating material, abrasion occurs along magnetic field lines. With the magnetic sputtering method, electrons are directed to ensure that collisions are closer to the cathode surface. In this region, they cause an increase in ionization and a denser plasma. With the increase of the ionization effect, magnetic fields that can generate plasma at lower operating pressures than the main sputtering systems can be created. By lowering the working pressure, the sputtering of the target atoms in the gas phase will be less, so the number of particles reaching the substrate increases and their deposition rate becomes relatively higher. As a result, with the effective use of electrons, coating can be made at low pressure (0.13-0.39 Pa) and low voltage (300-700 V).

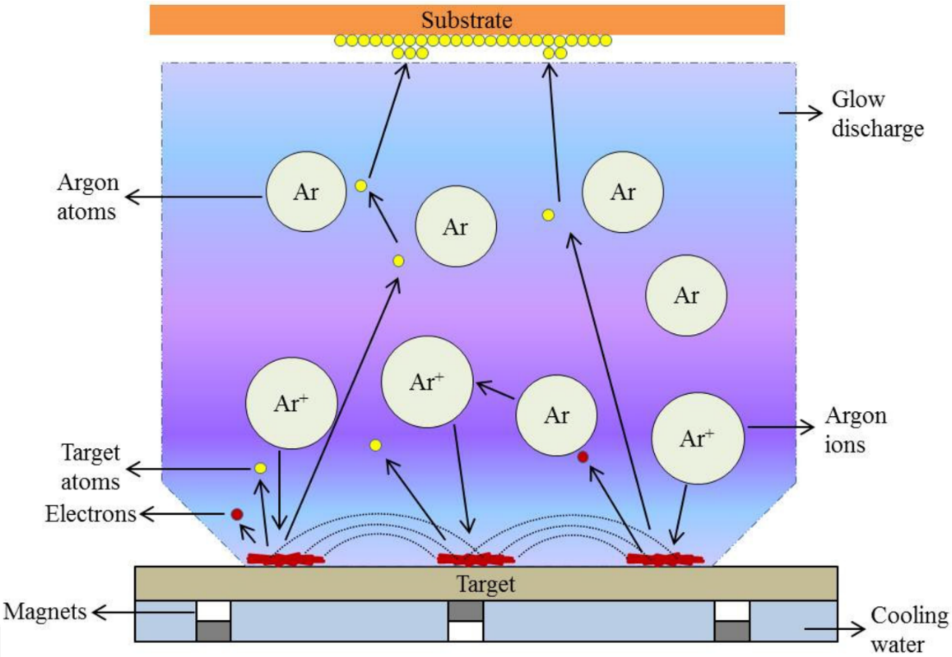

Figure 2.17 Magnetic sputtering mechanism (Maurya et al., 2014)

CHAPTER THREE
LITERATURE REVIEW

3.1 Optical Thin Films Effective in UV and IR Region

The world's most important and largest energy source is the sun. While this energy provides us with the heat and light we need, it also sends harmful UV rays. It is the wavelength of the incident beam that determines how this radiation affects us and how it is absorbed in different tissues. These tissues are especially those found in the eye and providing vision and those in the skin, and both are sensitive to the damage caused by UV rays. There are also many solar rays such as cosmic rays, gamma rays, X-rays, and radio frequency radiation, but they do not significantly affect our skin because they are present on earth in very small amounts or their energy is very low. According to the study conducted by Şahan et al. in 2015, the average solar energy density reaching a surface perpendicular to the arrival of sunlight at the upper limit of the atmosphere at a distance of 160 km from the earth's surface is approximately 1.37 kW m^2, which is called as "solar constant" and shown in Figure 3.1 (Şahan et al., 2015).

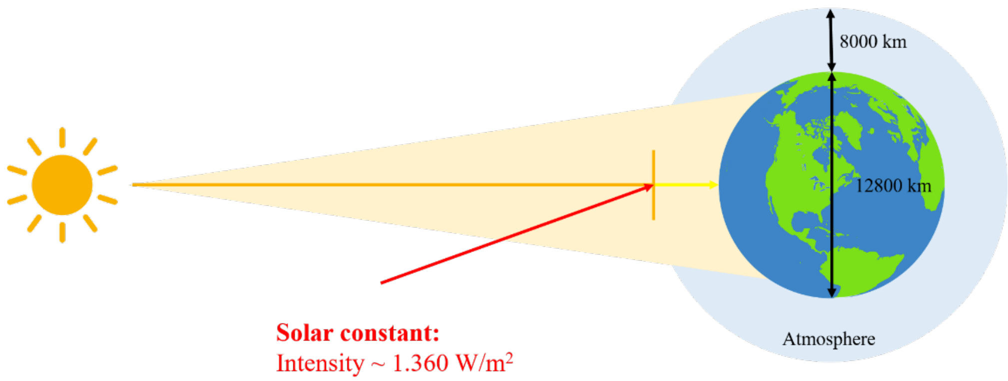

Figure 3.1 Schematic representation of the intensity (solar constant) of solar radiation directly outside the earth's atmosphere on a horizontal surface

The region that makes the best use of solar energy is the part of the equator between 35° north and south latitudes. This region is called the "Global Solar Belt". It receives 2000-3500 hours of sun in 1 year and its solar potential varies between 3.5-7 $kWh/m^2/day$. The average annual amount of solar radiation on earth varies between

2000-2500 kWh/m^2 in arid regions and 1000-1500 kWh/m^2 in higher latitudes. According to General Manager of Renewable Energy data, Turkey's total annual duration of sunshine 2640 hours (daily total of 7.2 hours), average total solar radiation is 1311 kWh/m^2/year (daily total of 3.6 kWh/m^2) that have been identified. Solar energy potential is calculated as 380 billion kWh/year.

On the subject of eliminating the harmful effects of UV rays on the human body, which is one of the efforts to find solutions to two important problems of the thesis;

Those that belong to the UV region from the sun's rays are divided into three as UV A, UV B and UV C. Of these, only UV A and UV B can reach the earth. The nature and amount of this type of radiation can vary depending on the events in the atmosphere. The degree of exposure to sunlight depends on many factors such as the amount of cloud, the ozone layer, the height of the sun, the geographical position of the location, occupation and related living conditions. Since UV light is harmful for the skin, some health problems occur in the human body. When human skin is exposed to UV rays with a certain wavelength due to its structure, it gives an acute reaction in the form of a burn. If this exposure occurs for a long time and periodically, sensitivity to sunlight, burns and acne formation on the skin, premature aging of the skin, wrinkle formation and even skin cancer may occur. Considering the amount of solar radiation in different parts of the world, it is seen that our country is highly likely to encounter UV-induced health problems. At the same time, since our country is located in the "Mediterranean Region Belt", it is the target of UV rays, especially in the summer months. Therefore, it is essential to be protected from UV rays both in terms of health and personal life comfort. In addition, skin cancer is the most common of all cancers and 90% of skin cancer cases are caused by harmful rays from the sun. In recent years, with the increase in the use of fluorocarbon compounds in coolant sprays or deodorants, the ozone layer has been thinned and this has led to more harmful effects of UV A and UV B rays.

The study by Miao et al. revealed that the clothes used in daily life do not adequately protect our bodies from the effects of UV rays. Within the scope of the study, the advantage of the air permeability and flexibility of textile products was emphasized, while the weak UV-reflecting feature was emphasized as a disadvantage (Miao et al., 2014). The necessity of modification on the textile surface to protect from UV rays was emphasized also in the study of Miao et al. in 2015. With this study, the UV light reflection rate of the textile surface was increased to 98% by using TiO_2 material (Miao et al., 2015).

In the study of Du et al. in 2012, some simulation programs were used to determine the absorption and reflection rates of the structures obtained by creating zinc oxide (ZnO) nanofibers and nano-cavities for the coating with reflective properties as an effective UV blocker. Compared to ZnO thin films, there has been an improvement in the performance of both fibers and nano-voids. ZnO nano fibers and voids have similar absorption in the UV range. However, ZnO nano fibers have lower absorption than nano-voids in the visible range. The effects of changes made by simulating different crystal parameters were analyzed. Optical properties of these nano-structured coatings provide UV reflection and wide contact angle (Du et al., 2012).

In the study of Houng & Chen in 2012, it was aimed to produce ZnO in a low cost, stable and environmentally friendly manner. For this purpose, aluminum is doped into the structure to reduce the resistivity value of the material. Thus, the UV reflective feature of the new material, which is formed by the increase of free electrons of the material and thus the increase in its conductivity, has also increased (Houng & Chen, 2012).

Another effort of the thesis to find a solution to two important problems is on preventing the detection of IR rays in thermal cameras by controlling the reflection of the human body;

In the study conducted by Jiang et al. in 2017, an Ag film with a thickness of 200 nm was coated on cotton and polyester fabric samples by magnetron sputtering method. The physical properties of the coated fabrics were evaluated by examining the IR reflectance / transmission rate and UV protection factor value. It was observed that the IR reflectance rate of the Ag coated fabrics was 30-35%, the IR emission value was about 0.7 and the maximum ultraviolet protection value (UPF) value was 218. According to the results, Ag coated fabrics provided excellent protection against UV radiation and good protection against IR radiation. In the study, it has been observed that Ag has a protective effect against UV and IR rays (Jiang et al., 2017).

In the study of Miao et al. in 2017, Cu and Ti films with a thickness of 200 nm were coated on cotton and polyester fabrics with magnetron sputtering technology. Among the physical properties of evaluated coated fabrics, IR emission, reflection rate, contact angle and UPF values were determined. Cu coated fabric samples were found to have 20-30% IR reflectance, about 0.7 IR emission value and 273 UPF. Cu coated fabric samples therefore have excellent UV and IR protection. It has been observed that these materials can be used for textiles providing protection from sunlight (Miao et al., 2017).

In the study of Jiang et al. in 2017, an aluminum-doped zinc oxide (AZO) film was coated on a polyester fabric by magnetron sputtering method. The results showed that the AZO coatings had a contact angle value of 14 ° and a UPF value of 362. In addition, the IR emission of AZO coated polyester fabric was reduced from 0.979 to 0.916 as a result of 450 nm coating (Jiang et al., 2017).

In a study published by Miao et al. in 2014, AZO / Ag / AZO three-layer films were coated on glass surfaces with RF magnetron sputtering technology. The electrical and infrared reflection properties of these three-layer structures were investigated by four-point probe system and Fourier Transform Infrared Spectroscopy (FTIR). The results showed that the Ag inner layer started to form a continuous film of 10 nm thickness. In addition, the highest apparent permeability of 80.5% was obtained with AZO (30nm)/Ag (10nm)/AZO (30nm) structure. The lowest layer resistance of 4.36 Ω/sq and the highest infrared reflection rate were achieved with 96% AZO (30nm)/Ag (13nm)/AZO (30nm) structure. The high infrared reflectivity of AZO/Ag/AZO three layers is considered promising for energy efficient coatings (Miao et al., 2014).

When the studies are examined, it is understood that the reflectance level of UV and IR rays of normal textile products is not sufficient. UV and IR protection can be provided by doping a conductive element or molecule into the transparent conductive oxide structure or by forming a TCO/ metal/TCO structure.

CHAPTER FOUR
EXPERIMENTAL PROCEDURE

4.1 Purpose

As mentioned in the previous chapters, functional thin films can be deposited optimally on textile substrates for UV protection and IR stealth applications via RF magnetron sputtering systems. In this thesis, various thin films with different configurations were deposited on polyester fabric substrates to determine the thin film with the best optical performance. Before the deposition process, oxygen plasma cleaning was applied to polyester fabrics and glass substrates. High purity commercial target materials were used to produce thin films. In addition to the textile coatings, which are the main purpose of the thesis, glass substrates were also coated to facilitate characterization. Finally, glass substrates and fabrics covered with sandwich-structured thin films were evaluated in detail using structural, chemical, morphological and optical characterization methods.

4.2 Materials

In this part, supplier information and physical, chemical and electrical properties of target materials used in thin film production were listed in the Table 4.1. Heat-releasing polyester fabrics and glass substrates were purchased from İltema (Turkey).

Table 4.1 Properties of target materials used

	TiO_2 Target	Al Target	Cu Target
Supplier	Kurt J. Lesker Company	Kurt J. Lesker Company	Kurt J. Lesker Company
Size	2.00" Dia. x 0.250" Thick	2.00" Dia. x 0.250" Thick	2.00" Dia. x 0.250" Thick
Purity	99.99%	99.99%	99.99%
Color	Gray to White	Silvery, Metallic	Copper, Metallic
Theoretical Density (g/cc)	4.23	2.7	8.92
Z Ratio	0.4	1.08	0.437
Max Power Density (Watts/Square Inch)	20	150	200
Image			

4.3 Methods

Commercially purchased target materials were used to deposit thin film in the RF magnetron sputtering system. Glass substrates were cleaned by standard procedure with ethanol (C_2H_5OH) and distilled water before being placed in the chamber. Later, pre-cleaned glass substrates and polyester fabrics cut in appropriate sizes were exposed to an oxygen plasma (Femto Science, CUTE) to increase coating adhesion. Oxygen plasma device was shown in Figure 4.1. The parameters of the oxygen plasma cleaning process were given in Table 4.2.

Figure 4.1 A photo of the oxygen plasma device (Personal archive, 2020)

Table 4.2 Parameters of oxygen plasma treatment

Plasma gas	Oxygen
Pressure	0.07 torr
Power	80 Watt
Gas flow	22 sccm
Time	3 min

The chamber of the RF Magnetron Sputter device (Nanovak NVTH-350, EMUM) (Fig. 4.2) was taken to vacuum after the substrate materials to be coated were placed in the sample holder. Details of parameters for all deposition conditions such as temperature, gas flow rates, power, and chamber gas pressure were shown in Table 4.3.

Figure 4.2 RF Magnetron Sputtering device (Personal archive, 2020)

Table 4.3 RF Sputtering parameters and conditions

Target	TiO_2	Cu	Al
RF Power	60 W	30 W	40 W
Base Vacuum	3- 4.5 x 10^{-6} Torr	3- 4.5 x 10^{-6} Torr	3- 4.5 x 10^{-6} Torr
Deposition Pressure	1.05 x 10^{-2} Torr	1.05 x 10^{-2} Torr	1.05 x 10^{-2} Torr
Gas Flow	31 sccm	28 sccm	29 sccm
Deposition Rate	0.0 – 0.1 Å/s	5 Å/s	5 Å/s
The Substrate to Target Distance	10 cm	10 cm	10 cm
Substrate Temperature	298 K	298 K	298 K

Cu and Al layers were deposited at different times (40 s - 90 s) to examine the effect of thin-film thickness on optical properties. TiO_2 layer was deposited first to increase the adhesion of the metal Cu layer on the glass substrate. After the formation of Cu and Al based metallic coatings, TiO_2 was again deposited on the top to prevent corrosion and oxidation (TiO_2/Cu-Al/TiO_2). The schematic structure of the coatings on the fabric is shown in the Figure 4.3. All samples were named depending on the deposition time applied and given in Table 4.4.

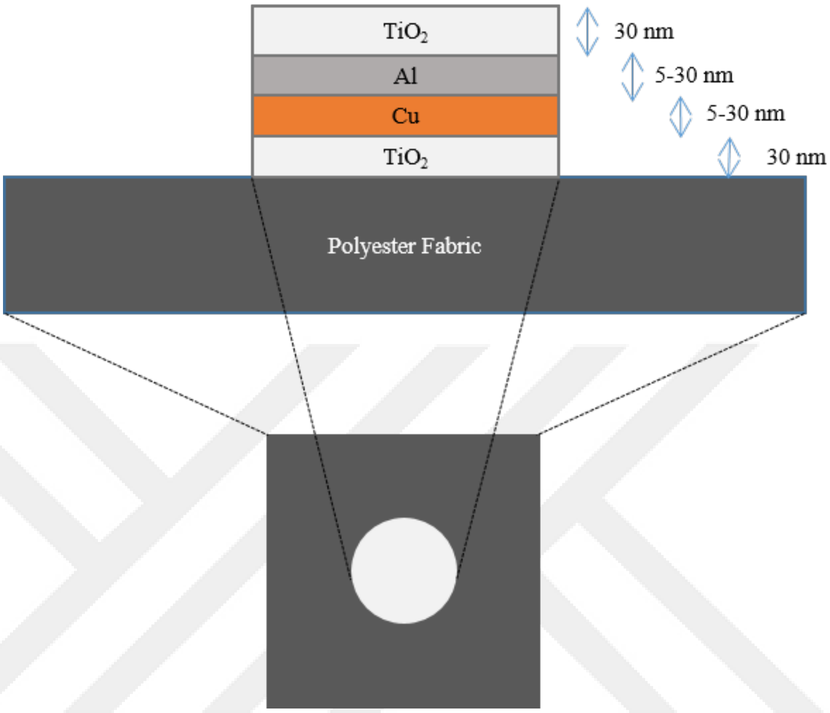

Figure 4.3 The schematic structure of the coatings on the fabric

Table 4.4 Deposition times and naming of samples

		Deposition Times			
Sample Names		**TiO_2 (Bottom)**	**Cu**	**Al**	**TiO_2 (Top)**
	TC4A9T	1 h	40 s	90 s	1 h
	TC5A8T	1 h	50 s	80 s	1 h
	TC6A7T	1 h	60 s	70 s	1 h
	TC7A6T	1 h	70 s	60 s	1 h
	TC8A5T	1 h	80 s	50 s	1 h
	TC9A4T	1 h	90 s	40 s	1 h

4.4 Materials Characterization

4.4.1 X-Ray Diffraction

X-ray diffraction (XRD) analysis, which is a very effective technique, is used to determine the crystal phases of powders or films. In addition, it can be used to analyze the crystalline grain size, tension, phase composition, and crystal orientation of materials. It simply changes the angle of the incident beam and sends it to the material and makes it possible to obtain a pattern of the resulting diffraction angle (2θ) values.

After thin films were deposited on glass substrates and polyester fabrics, XRD measurements were performed. Thermo Scientific's ARL X'TRA model device was used to obtain XRD patterns (as depicted in Fig. 4.4). Cu-Kα (1.54185 Å) radiation was used at 40 kV and 40 mA to determine the crystal structures of the samples, and scanning was performed between 2θ of 5°-90° at room temperature. Scanning was performed for all samples at a scanning rate of 4°/min.

Figure 4.4 X-Ray Diffractometer, Thermoscientific ARL X’TRA (Personal archive, 2020)

4.4.2 Scanning Electron Microscopy

Scanning electron microscopy (SEM) is an analytical method commonly used to study the surface morphology of solid-state samples. An electron beam of high energy and a narrow diameter scans the surface of the sample in SEM analysis. In addition, elemental analysis can be performed using the radiation resulting from the interaction between the electron beam and the sample.

As the electron interacts with the surface, secondary electrons (SE), backscattered electrons (BSE) and characteristic X-rays are obtained. The electrons that result from the interaction of an electron with atoms on the surface of the sample are called SE. The high-resolution images obtained using this resulting SE are used for morphological characterization of the material surface. SEM analysis supports obtaining a characteristic three-dimensional (3D) surface view because it uses a very narrow beam of electron beams for imaging and the images have a wide depth of field. Theoretically, high magnifications such as hundreds of thousand times magnification can be obtained.

Electrons reflected back by elastic scattering from sample surfaces are called BSE. By using the strong relationship between the atomic number of the elements on the surface and the BSE signal intensities, comments can be made about the distribution of the different elements on the material surface. While making this interpretation, different concentration regions belonging to different phases obtained in the images are examined.

When the primary electron hits the surface of the material being characterized, an electron can be excited from the inner shell. As a result of the excitation, a characteristic X-ray emission occurs, which is equal to the energy difference between the electron orbits. Using these X-ray measurements, the composition and amounts of elements in the sample are measured.

SEM device (Zeiss, Gemini) was used to examine the surface morphology of thin films using SE at 10-13 kV applied voltage (as presented in Fig. 4.5). The magnification used for analysis is 500x.

Figure 4.5 Zeiss Gemini model SEM device (Personal archive, 2020)

4.4.3 X-Ray Photoelectron Spectroscopy

With X-ray photoelectron spectroscopy (XPS), the elemental composition, chemical state, and electronic state of a material can be quantitatively determined. X-rays are directed to the material surface and simultaneously the kinetic energy and the number of electrons are measured from a depth of 1 to 10 nm of the sample surface. Ultra-high vacuum (UHV) condition is absolutely necessary for XPS analysis.

XPS analysis can be used to analyze the surface chemistry of the sample. It can also be used to characterize the effects of mechanical deformation processes or the effects of ion beam etching, solutions, beam implant and ultraviolet light. Hydrogen (H) and helium (He) cannot be detected due to the very small diameter of orbitals, while all elements with atomic number equal to or higher than 3 (lithium, Li) can be detected by XPS analysis. A Thermo Scientific K-Alpha device with a monochromatic Al-Kα (1486.7 eV) X-ray source was used for XPS analysis (as depicted in Fig. 4.6). The purpose of the XPS was to analyze the chemical presence of sandwich structure thin film coatings and their successful overlapping in the desired order. For this purpose, depth profile analysis was performed with 2000 eV high current ion power for 40 s periods on the coatings on the glass surface produced within the scope of the thesis.

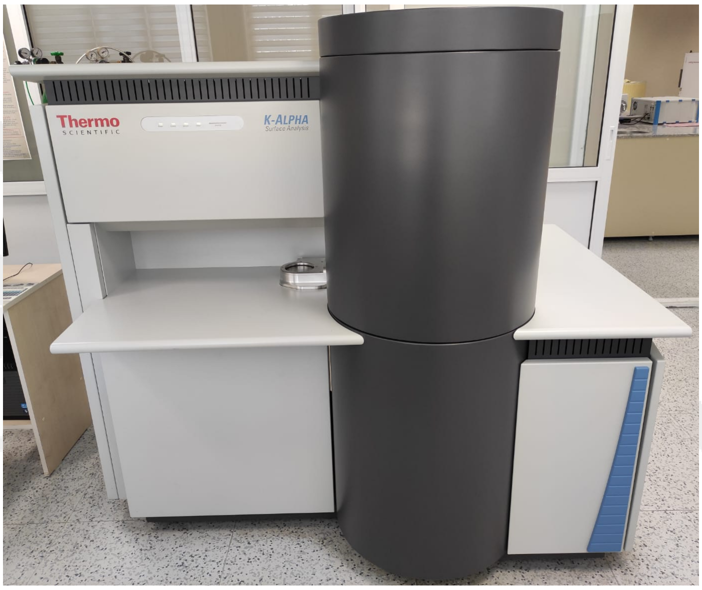

Figure 4.6 Thermo Scientific K-Alpha XPS device (Personal archive, 2020)

4.4.4 UV/VIS/NIR Spectroscopy

Optical characterization of the produced samples was carried out with a UV/VIS/NIR spectrophotometer (Perkin Elmer, Lambda 950) presented in Figure 4.7. UV/VIS/NIR spectrophotometer is used to determine the reflection, absorbance or transmittance properties of materials according to wavelength, especially in the visible range. UV/VIS/NIR spectrophotometer analysis was used to examine the optical properties of polyester fabrics coated with sandwich structured thin films. The data obtained were transferred to separate graphics for three different regions.

Figure 4.7 Perkin Elmer, Lambda 950 UV/VIS/NIR spectrophotometer device (Personal archive, 2020)

4.4.5 *Fourier Transform Infrared Spectroscopy*

Fourier Transform Infrared Spectroscopy (FTIR) is used for the analysis of chemical bonds and functional groups, especially in the structure of organic materials. Due to the different combination of atoms for each material, two different compounds always show different infrared spectra. These spectra are unique and unchanging for each material. Hence the FTIR spectrum is like a fingerprint for the material. Chemical bonds in the molecular structure of a material can be detected by evaluating the infrared absorbance and transmittance spectrum obtained by FTIR analysis.

Depending on the type and structure of the bonds and elements, chemical bonds vibrate at various frequencies. With the absorption of light energy, the bond is stimulated and the vibration frequency increases.

The Thermo scientific NICOLET iS10 FTIR instrument shown in the Figure 4.8 was used to characterize the chemical bonds of samples in the 400-4000 cm^{-1} range. Infrared reflection rate graphs were obtained by converting the obtained transmittance spectra into reflectance data.

Figure 4.8 Image of the used FTIR device having ATR apparatus (Personal archive, 2021)

4.4.6 Thermal Camera

Thermal imaging of polyester fabrics with heat releasing properties covered with sandwich-structured thin films was performed with the help of a thermal camera as presented in Figure 4.9 (Fluke, Ti27).

Figure 4.9 Fluke, Ti27 thermal camera (Personal archive, 2020)

The photo of one of the samples is given in Figure 4.10. Thermal imaging was done in two ways, areal and linear. Before the linear imaging, 12 V potential was applied to the ends of the carbon fiber passing through the middle of the samples for 30 s with the help of a power source (TT Technic, RXN–605D) in order to warm the fabrics. For areal imaging, a hot plate was heated to 40°C and the coated fabrics were placed on this plate. In the same way as the linear measurement, it was waited for 30 s and the thermal camera images were taken.

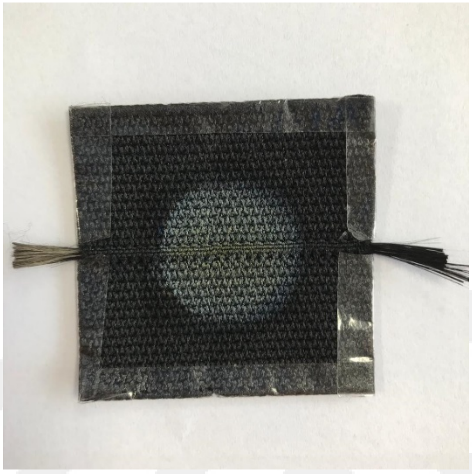

Figure 4.10 One of the TiO_2/Cu-Al/TiO_2 based thin films deposited by RF magnetron sputtering technique on polyester fabrics (Personal archive, 2020)

CHAPTER FIVE
RESULTS AND DISCUSSION

5.1 Structural Properties

The XRD graphs of TiO_2/Cu-Al/TiO_2 based thin films deposited on glass substrates (produced as a control sample for characterization) were given in Figure 5.1. Since no heat treatment was applied to the thin films deposited substrates before the XRD analysis, no crystalline peak of the amorphous glass substrates and TiO_2 was observed (Zhao et al., 2004). The peaks at 43.4°, 50.3°, and 74.1° which are related to the following planes (111), (200), and (220), respectively belong to the Cu thin film (Akkari et al., 2007). It shows a good agreement with the JCPDS card no. 01-085-1326 of Cu (Giroire et al., 2017). However, peaks at 38.4°, 44.7°, 65.1°, and 78.2° are related to the planes (111), (200), (220) and (311) of Al, respectively (Smecca et al., 2015). Also, it shows a good agreement with the JCPDS card no 00-004-0787 of Al (Shi et al., 2010).

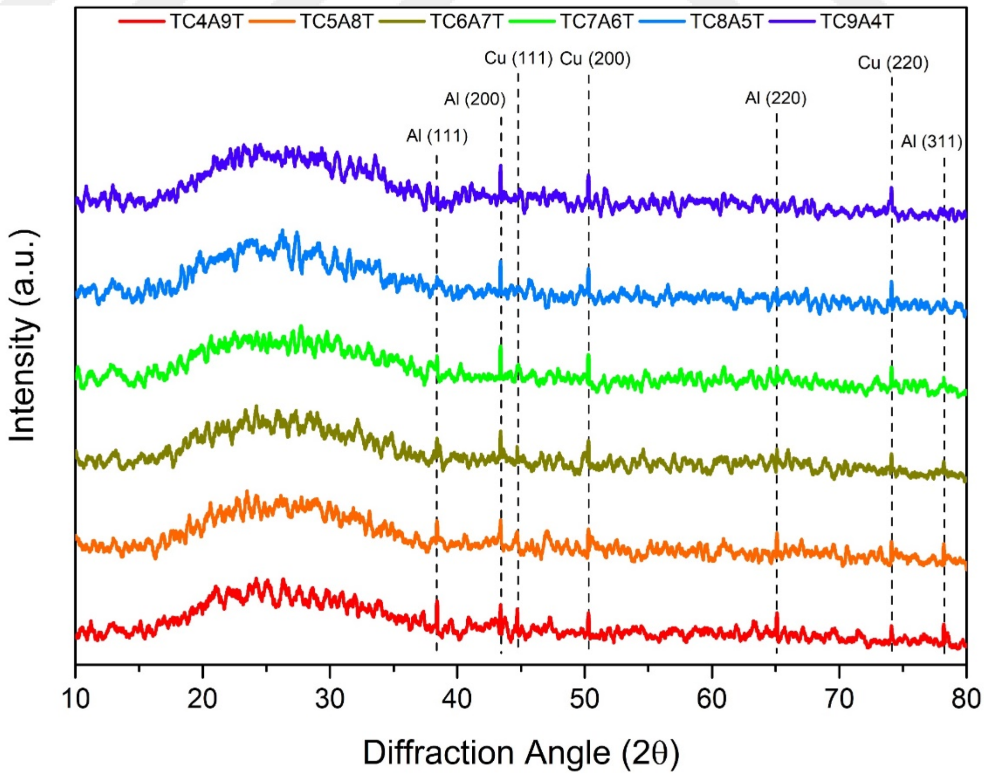

Figure 5.1 XRD graphs of TiO_2/Cu-Al/TiO_2 thin films deposited on the glass substrates

5.2 Morphological Properties

The SEM images of TiO_2/Cu-Al/TiO_2 based thin films deposited on glass substrates with RF magnetron sputtering system were given in Figure 5.2. When the images of produced thin films were examined, it is seen that the films were coated homogeneously but have some impurities. The reason for the impurities and heterogeneous zones can be cited as the magnetron sputtering device's chamber not being fully cleaned prior to production, the films being used as prepared, and not subjected to heat treatment.

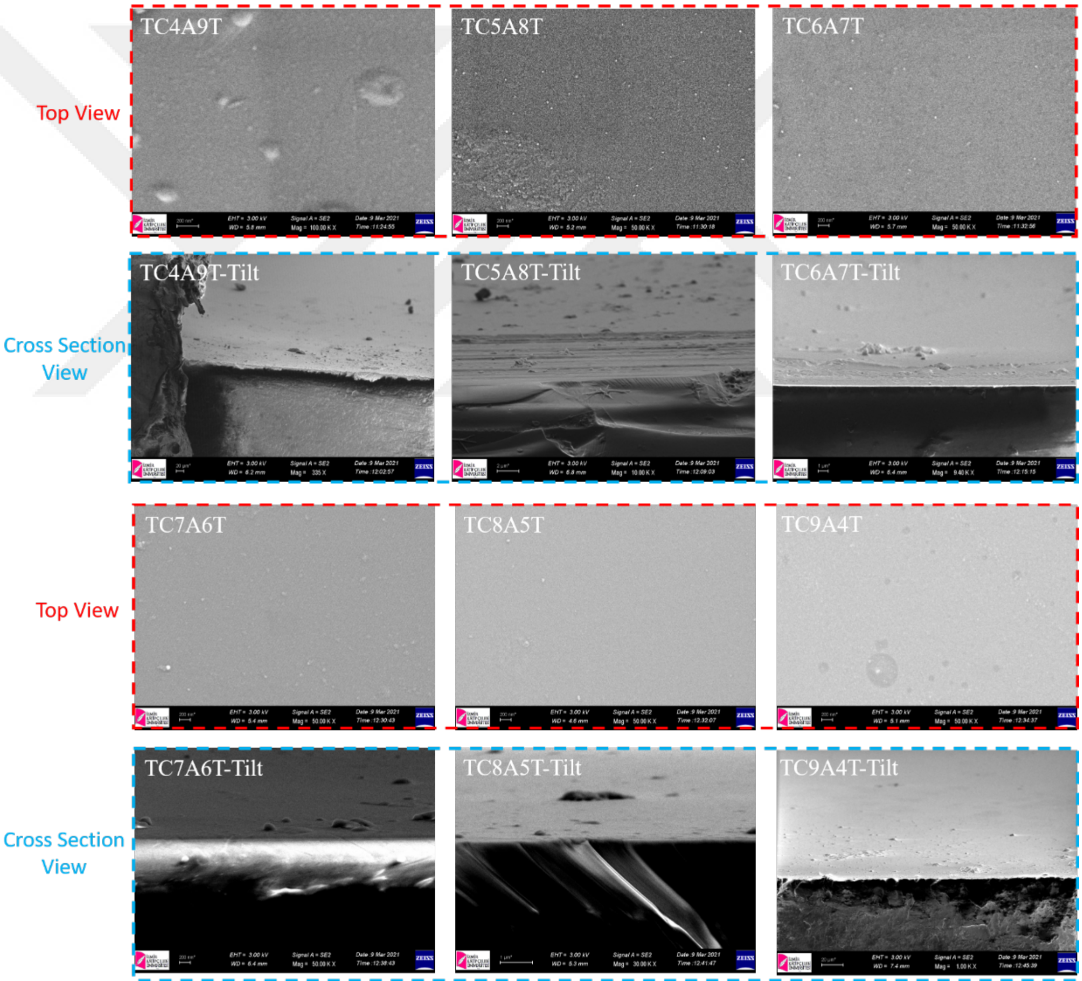

Figure 5.2 SEM images of the TiO_2/Cu-Al/TiO_2 samples deposited on glass substrates at 500x magnification

The Figure 5.3 shows the images of the samples covered with the TiO_2/Cu-Al/TiO_2 structure. When the Figure 5.3 is examined, it is seen that the fibers of polyester fabrics are covered homogeneously. When the photos at 2.5k magnification are examined in detail, the layered coating structure can be clearly seen. In addition, it was observed that the coating was discontinuous in some regions. This may be due to the fact that the coating application is carried out in a very short time and the substrate material has a fibrous structure containing voids.

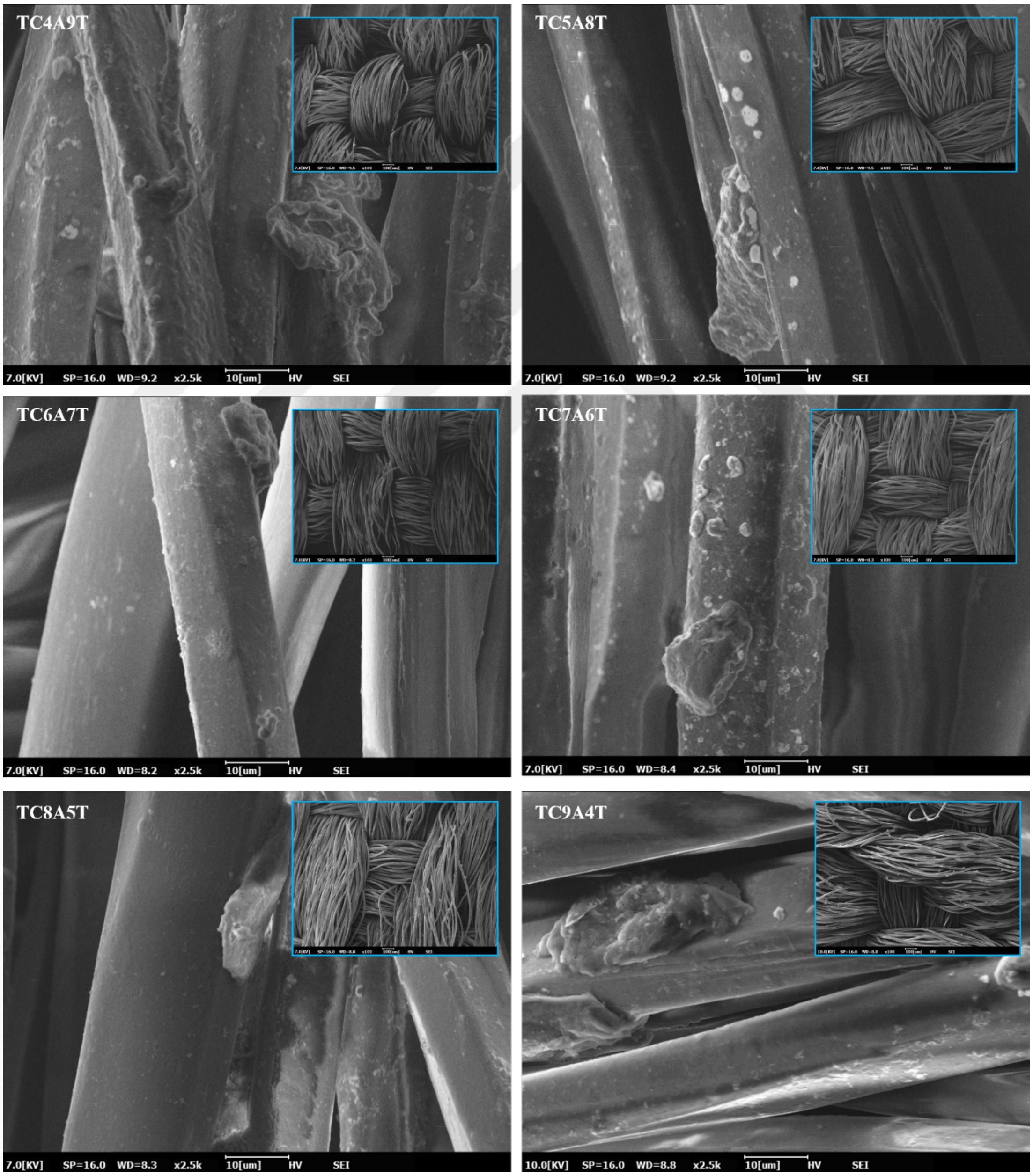

Figure 5.3 SEM images of TiO_2/Cu-Al/TiO_2 coatings deposited on polyester fabrics; main view at x2.5k, inner view at x100

5.3 Chemical Properties

The elemental mapping was carried out from the wide survey spectra of TiO_2, Cu, and Al-based monolayer films (named with element name and number from 4 to 9 representing 40 sec to 90 sec) measured over a binding energy range of 0 to 1350 eV, and the graph is displayed in Figure 5.4. A standard carbon peak C1s at 284.80 eV was observed in the spectra as the reference peak for all the samples. The spectra of TiO_2 monolayer coated glass includes Ti2p, C1s, and O1s peaks. There are no other fundamental peaks in the spectra, which clearly indicates that the deposited films do not contain any foreign elements in the sample. The spectra of Cu monolayer coated glass include Cu2p, O1s, C1s, and Na1s peaks, while Al monolayer coated glass contains Al2p, O1s, C1s, and Na1s peaks. It was decided that Na1s and O1s peaks come from the used substrate because the used substrate was soda-lime glass. The binding energies, FWHM values and detailed chemical properties of the peaks of the elements in all samples are given in the Table 5.1, 5.2, and 5.3.

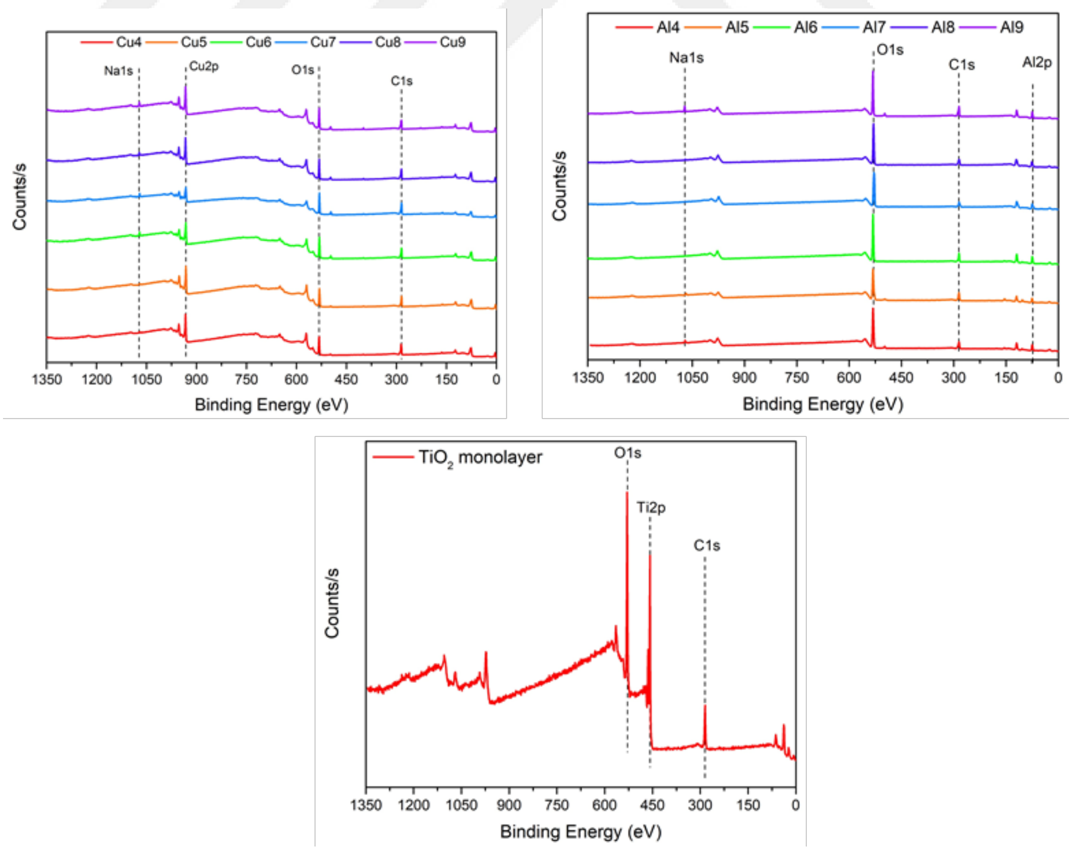

Figure 5.4 Wide survey XPS spectra of monolayered thin films

Table 5.1 The binding energies, FWHM values and detailed chemical properties of the peaks of the elements in TiO_2 monolayer sample

	Name	Peak (eV)	FWHM	Details
TiO_2 monolayer	Ti2p	457.66	1.49	Metal oxide – TiO_2
	C1s	284.55	2.06	C-C or C-H
	O1s	528.90	1.69	Metal oxide

Table 5.2 The binding energies, FWHM values and detailed chemical properties of the peaks of the elements in Cu samples

	Name	Peak (eV)	FWHM	Details
Cu4	Cu2p	930.21	1.42	Cu_2O, element
	O1s	530.97	2.39	Metal CO_3
	C1s	284.07	2.86	C-C or C-H, carbonate
	Na1s	1069.13	2.42	Element
Cu5	Cu2p	930.24	1.47	Cu_2O, element
	O1s	529.59	2.51	Metal oxide
	C1s	282.98	1.74	C-C or C-H, carbonate
	Na1s	1069.35	1.79	Element
Cu6	Cu2p	931.28	1.54	Cu_2O, element
	O1s	530.56	2.14	Metal oxide
	C1s	283.89	1.99	C-C or C-H, carbonate
	Na1s	1070.27	1.68	Element
Cu7	Cu2p	931.50	2.00	CuO, Cu_2O, element
	O1s	530.71	1.88	Metal oxide, metal CO_3
	C1s	284.01	1.93	C-C or C-H, carbonate
	Na1s	1070.32	1.74	Element
Cu8	Cu2p	932.49	1.53	CuO, Cu_2O, element
	O1s	531.53	2.18	Metal oxide, metal CO_3
	C1s	284.89	1.79	C-C or C-H, carbonate
	Na1s	1071.42	1.71	Element
Cu9	Cu2p	931.42	1.66	CuO, Cu_2O, element
	O1s	531.10	2.13	Metal oxide, metal CO_3
	C1s	284.74	1.85	C-C or C-H, carbonate
	Na1s	1070.26	1.72	Element

Table 5.3 The binding energies, FWHM values and detailed chemical properties of the peaks of the elements in Al samples

	Name	Peak (eV)	FWHM	Details
Al4	Al2p	74.84	2.67	Al_2O_3, element
	O1s	531.62	3.22	Metal oxide, metal CO_3
	C1s	285.29	2.69	C-C or C-H, carbonate
	Na1s	1069.74	2.24	Element
Al5	Al2p	76.25	2.23	Al_2O_3, element
	O1s	530.92	2.85	Metal oxide, metal CO_3
	C1s	285.37	2.05	C-C or C-H, carbonate
	Na1s	1068.70	1.92	Element
Al6	Al2p	73.15	1.80	Al_2O_3, element
	O1s	530.20	2.67	Metal oxide, metal CO_3
	C1s	283.48	1.59	C-C or C-H, carbonate
Al7	Al2p	74.79	2.22	Al_2O_3, element
	O1s	531.55	2.64	Metal oxide, metal CO_3
	C1s	285.05	1.92	C-C or C-H, carbonate
Al8	Al2p	74.96	2.34	Al_2O_3, element
	O1s	531.60	2.64	Metal oxide, metal CO_3
	C1s	285.13	1.98	C-C or C-H, carbonate
	Na1s	1071.35	1.99	Element
Al9	Al2p	74.29	1.79	Al_2O_3, element
	O1s	531.51	2.45	Metal oxide, metal CO_3
	C1s	284.61	1.66	C-C or C-H, carbonate
	Na1s	1071.56	1.80	Element

When Figure 5.5 is examined, while Cu2p and Al2p are not seen during the ion-etching period up to 120 s, Ti2p and O1s are seen. The presence of these elements is due to the TiO_2 layer applied to the top to protect the metal layers from corrosion and oxidation. Thanks to the increasing atomic weight percentages of Cu2p and Al2p from 120 s up to 200 s, the existence of metallic layers is clearly seen. In addition, the reduction of Ti2p and O1s peaks here indicates that the TiO_2 layer disappears after 120 s of ion-etching and the metallic layer is now reached. After 280 s of ion-etching, while the atomic weight percentages of Cu2p and Al2p decrease again, the atomic weight percentages of Ti2p and O1s increase which comes from the bottom TiO_2 layer applied to increase the adhesion of metals to the substrate. In the TC4A9T sample, the peak of Cu2p cannot be seen and the presence of high O1s peak is that the Cu thin film thickness is very low and ion etching reaches the glass substrate in a short time by completely etching the thin film. The high proportion of O1s is due to the O portion of SiO_2 in the glass substrate.

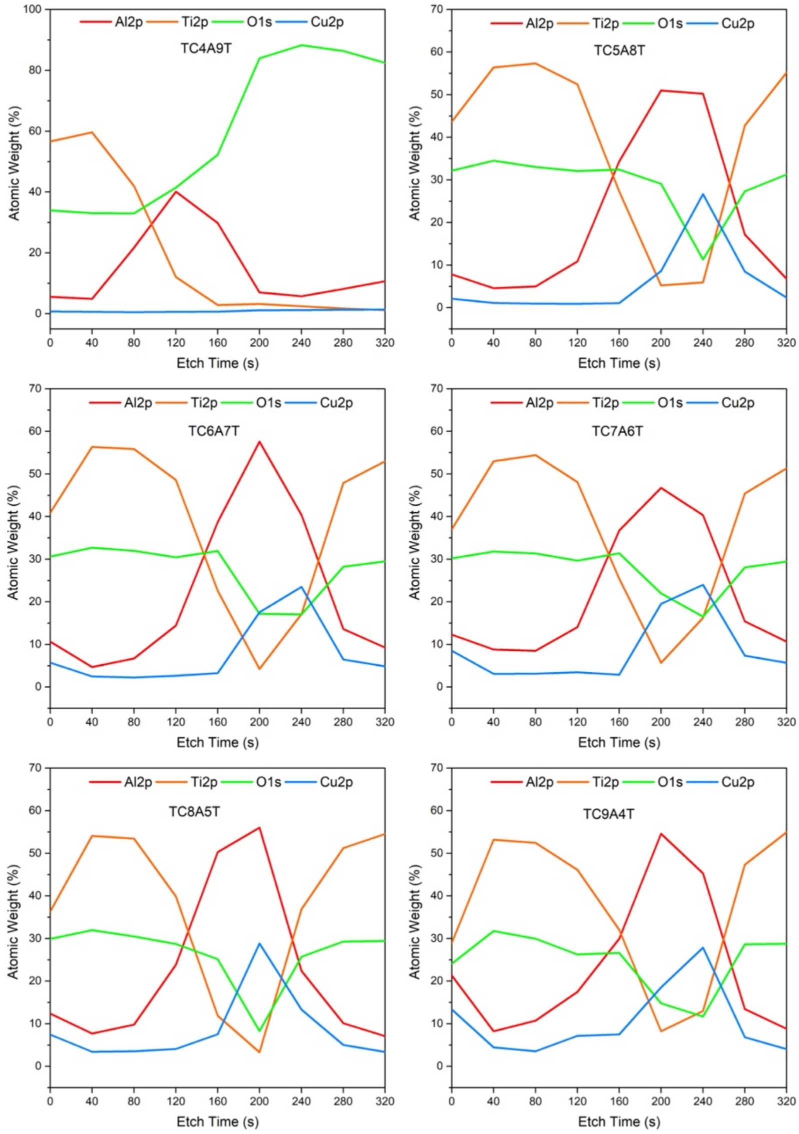

Figure 5.5 XPS depth profiles of TiO_2/Cu-Al/TiO_2 thin films deposited on the glass substrates

5.4 Optical Properties

The optical transmittance spectra of TiO_2/Cu-Al/TiO_2 samples are shown in Figure 5.6. As shown in the figure, the highest visible transmittance of the samples was obtained at the TC4A9T sample. The highest visible transmittance of TiO_2/Cu-Al/TiO_2

thin films was found as around 94%. The optical properties can be attributed to the sequence and thickness of the films. Because of the high transmittance in the visible area, the coatings will remain as a transparent layer in the area where they are applied. This situation greatly increases the applicability of the coating in many areas.

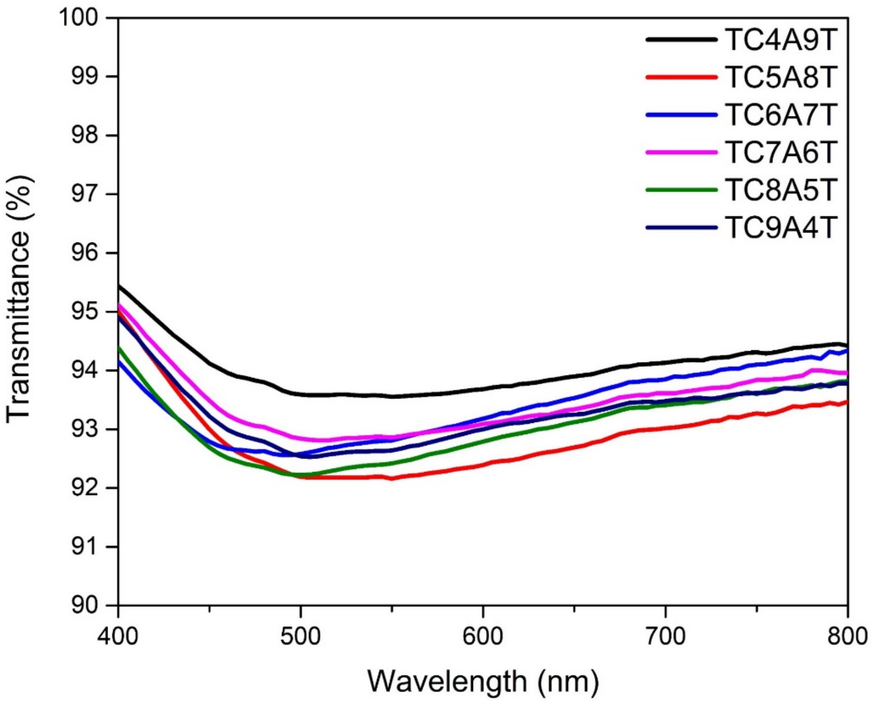

Figure 5.6 Optical reflectance spectra of TiO_2/Cu-Al/TiO_2 coated samples

The UV penetration rate is a critical factor that determines the UV protection properties of textiles. The protection abilities of the TiO_2/Cu-Al/TiO_2 thin film coated polyester fabrics from UV irradiation were tested. The UV transmittance spectra of the samples are shown in Figure 5.7. Higher UV transmittance means poor UV protection, while all samples show low UV transmittance. This shows that the coatings are very effective in UV protection due to the UV absorption ability of TiO_2, Cu, and Al. However, the UV transmittance of the coated fabric is significantly reduced at the TC6A7T sample which offers the best UV protection. Additionally, it can be seen that all of the TiO_2/Cu-Al/TiO_2 coated fabric samples show great UV protection due to a 10% UV transmittance.

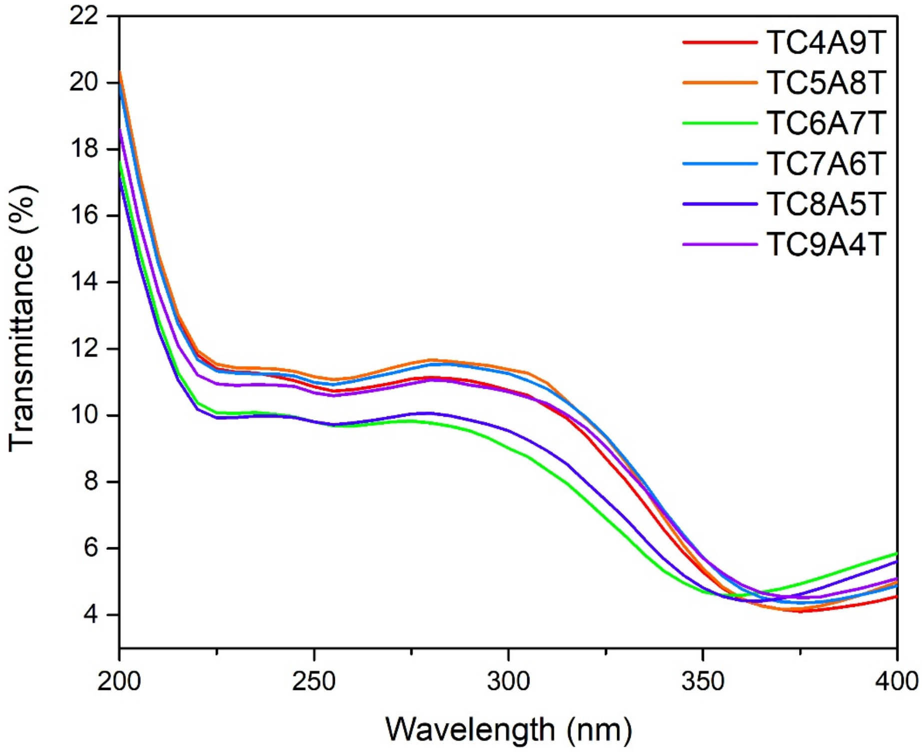

Figure 5.7 UV transmittance spectra of TiO_2/Cu-Al/TiO_2 coated polyester fabrics

5.5 Infrared Reflection Properties

The transmittance versus wavelength graphs of TiO_2/Cu-Al/TiO_2 based thin films deposited polyester fabrics were obtained in the range of 2.5 - 25 µm and is shown in Figure 5.8. When the graphics were examined, it was seen that the peaks for all samples were in the same regions. This indicates that there are no impurities or differences in the samples.

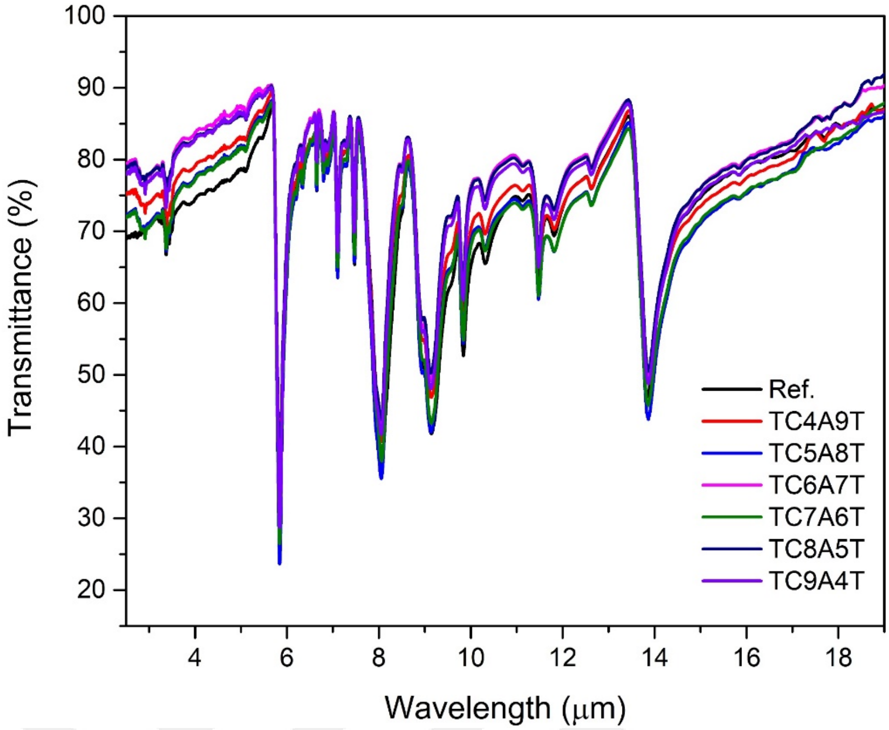

Figure 5.8 Transmittance spectra of TiO_2/Cu-Al/TiO_2 coated polyester fabrics in the range of 2.5 – 25 μm

By converting to transmission graphs, infrared reflection rate graphs were obtained and shown in the Figure 5.9. In order to make a more detailed comparison, polynomial fitting was applied to the infrared reflection rate graphics and presented in the Figure 5.10. When all the graphics were examined, it was determined that the TC5A8T sample was the best sample in terms of reflecting infrared light in the 2.5 - 25 μm range.

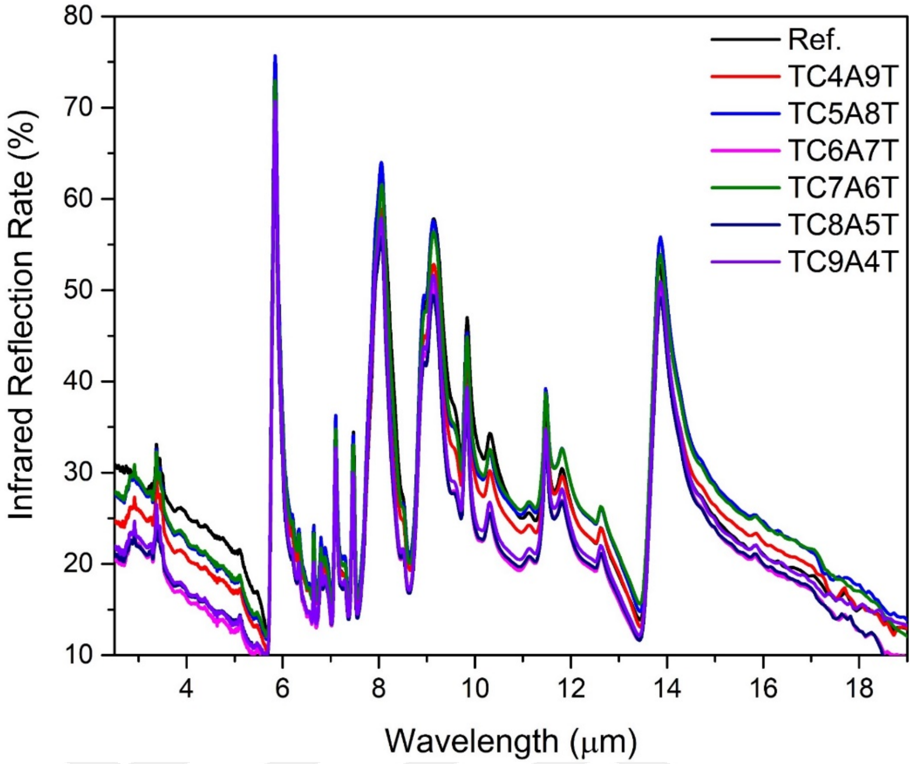

Figure 5.9 Infrared reflection rate graphs of TiO_2/Cu-Al/TiO_2 coated polyester fabrics in the range of 2.5 – 25 μm

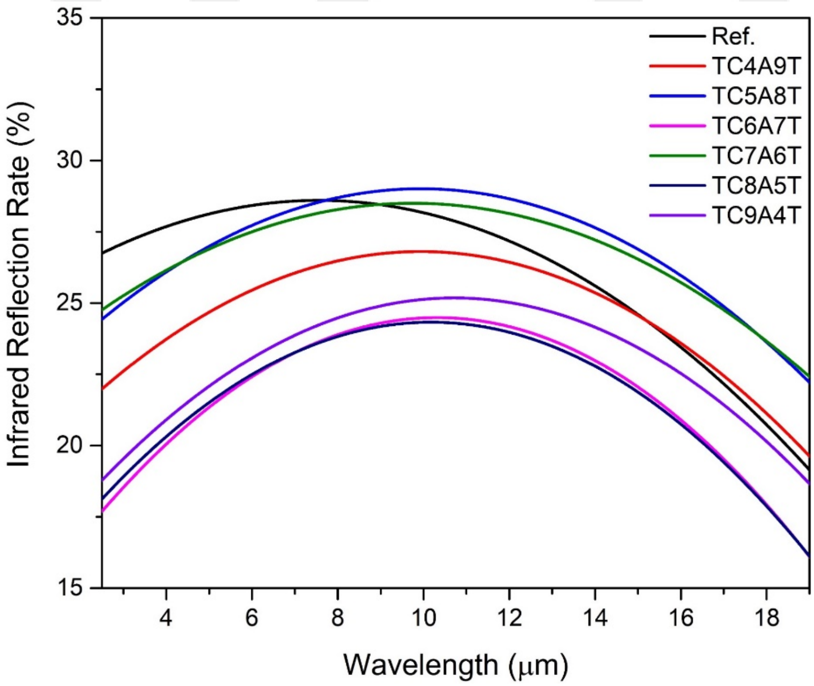

Figure 5.10 Curves of infrared reflection rate spectra obtained by applying polynomial fitting for TiO_2/Cu-Al/TiO_2 coated polyester fabric samples

5.6 Thermographic Properties

The thermal camera images of TiO_2/Cu-Al/TiO_2 based thin films deposited on heat-releasing polyester textiles were given in Figure 5.11 and 5.12. The thermographic properties were examined in Figure 5.11 in an areal way and in Figure 5.12 in a linear way. When the temperature scale in the images is examined, it is seen that the temperature of the environment where the photos were taken is around 42°C. This temperature is more than enough to examine the studies of preventing the reflection of human body temperature, which is one of the aims of the thesis, since the average human body temperature is 37°C. When all samples are examined, it is clearly seen that the coated region in the sample named TC5A8T has the lowest temperature value with 35°C. The reason for this is the different thickness values resulting from the deposition of Cu and Al at different times. The localized surface plasmon formed in Cu and Al layers of different thicknesses and between these layers have created variable effects in the direction of IR light. The thickness of the Cu layer in the TC5A8T sample was less than the others, while the higher Al layer thickness shows that the localized surface resonance was the best in this sample in terms of thermographic performance.

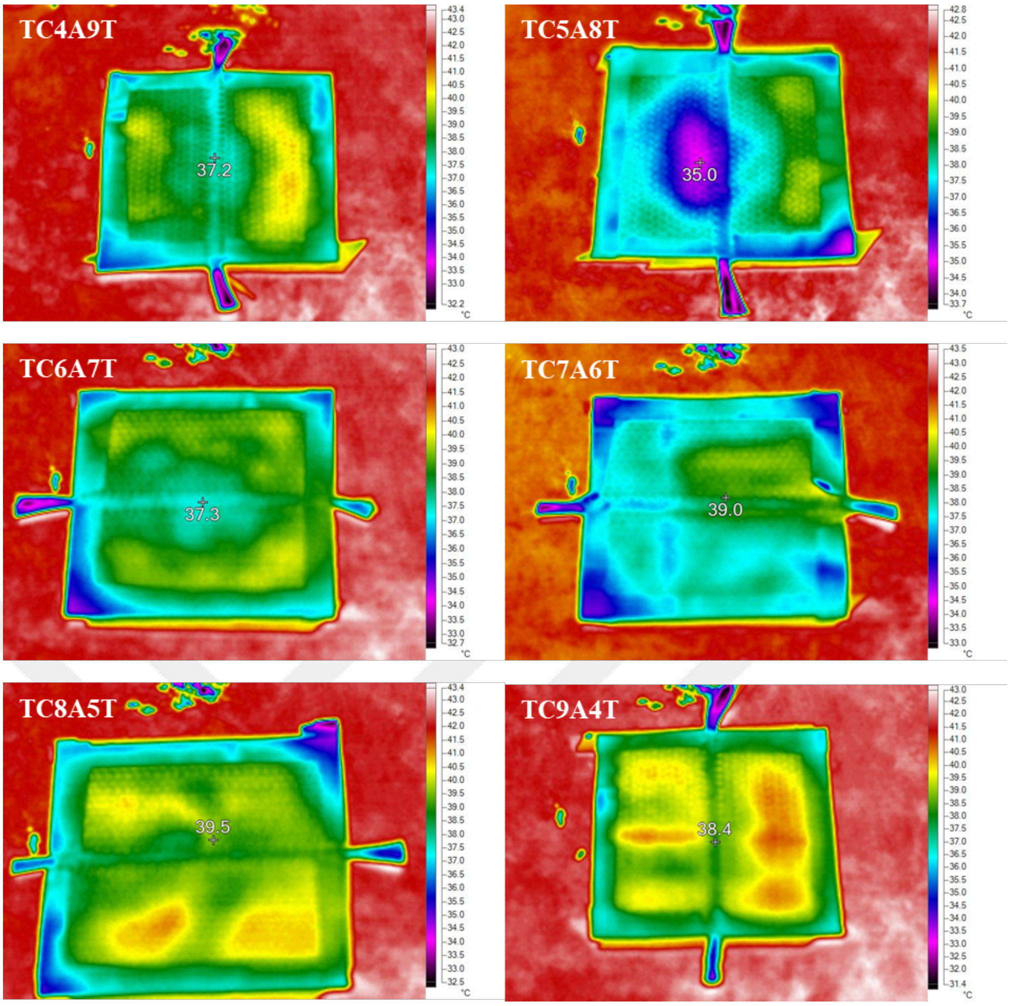

Figure 5.11 Thermal camera images taken over the entire surface of the TiO_2/Cu-Al/TiO_2 thin film coated polyester textiles for areal investigation of thermographic properties

The supplied heat-releasing polyester fabric takes this feature from the carbon fiber network passing through it. When a low amount of electrical potential is applied to the carbon fiber network from both ends, it can reach very high temperatures in a short time. When Figure 5.12 is examined, it is clearly seen that after electrical potential is applied to the carbon fiber, its ends rise above 100°C, but the middle zone is at relatively lower temperatures. Thus, the coating appears to be effective in preventing heat reflection and in terms of infrared stealth. It is understood that the sample exhibiting the most effective performance in this regard is the TC5A8T sample with a temperature value of approximately 76°C, as in the areal examination.

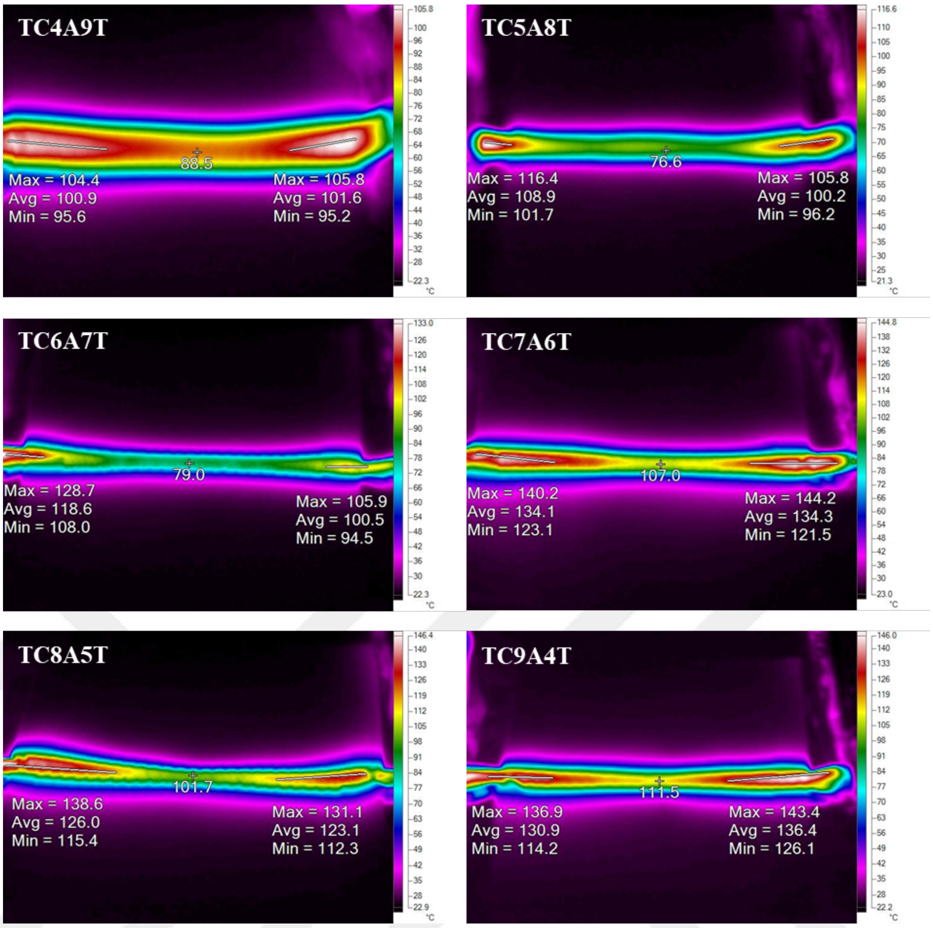

Figure 5.12 Thermal camera images taken from the carbon fibre region passing through the TiO_2/Cu-Al/TiO_2 thin film coated polyester textiles

CHAPTER SIX
CONCLUSION AND FUTURE WORKS

TiO_2/Cu-Al/TiO_2 sandwich sequenced heterogeneous structured thin films produced successfully by the RF magnetron sputtering technique on glass substrates and polyester fabrics. Obtained results are summarized as follows;

1. Magnetron sputtering parameters widely studied and optimum sputtering parameters have found for TiO_2, Cu, and Al targets.

2. All thin film coatings have an amorphous TiO_2 phase according to the XRD results while Cu and Al crystalline.

3. All thin film coatings have homogeneous and smooth coating surfaces with minor impurities.

4. Chemically, the presence of TiO_2, Cu, and Al was confirmed by XPS analysis. Moreover, it was proved by using the depth profile method in XPS analysis that the sandwich structure was successfully created.

5. The proposed TiO_2/Cu-Al/TiO_2 sandwich sequenced heterogeneous structure exhibited sunlight management properties.

6. The most effective coating on textile in reflecting UV and IR light irradiation was determined as TC5A8T sample.

The surface plasmon effect is related to the conductivity and thickness of the conductive layer. It has been shown that UV protection and IR stealth performance can be modified by the coating time (hence the coating thickness). The order of the coatings can be changed for better performance. Functional performance can be improved by applying heat treatment to coatings.

REFERENCES

Akkari, F. C., Kanzari, M., & Rezig, B. (2007). Preparation and characterization of obliquely deposited copper oxide thin films. *EPJ Applied Physics*, *40*(1), 49–54.

Arbab, E. A. A., & Mola, G. T. (2019). Metals decorated nanocomposite assisted charge transport in polymer solar cell. *Materials Science in Semiconductor Processing*, *91*, 1–8.

Badri, S. H., & Gilarlue, M. M. (2020). Coupling Si3N4 waveguide to SOI waveguide using transformation optics. *Optics Communications*, *460*, 125089.

Birkholz, M., Ehwald, K. E., Wolansky, D., Costina, I., Baristiran-Kaynak, C., Fröhlich, M., Beyer, H., Kapp, A., & Lisdat, F. (2010). Corrosion-resistant metal layers from a CMOS process for bioelectronic applications. *Surface and Coatings Technology*, *204*(12–13), 2055–2059.

Bobinger, M., Angeli, D., Colasanti, S., La Torraca, P., Larcher, L., & Lugli, P. (2017). Infrared, transient thermal, and electrical properties of silver nanowire thin films for transparent heaters and energy-efficient coatings. *Physica Status Solidi (A) Applications and Materials Science*, *214*(1), 1600466.

Budinovskii, S. A., Matveev, P. V., Smirnov, A. A., & Chubarov, D. A. (2019). Thermal-barrier coatings with an external magnetron-sputtered ceramic layer for high-temperature nickel alloy turbine blades. *Russian Metallurgy (Metally)*, *2019*(6), 617–623.

Chiarello, G. L., Bernareggi, M., Pedroni, M., Magni, M., Pietralunga, S. M., Tagliaferri, A., Vassallo, E., & Selli, E. (2017). Enhanced photopromoted electron transfer over a bilayer WO3 n-n heterojunction prepared by RF diode sputtering. *Journal of Materials Chemistry A*, *5*(25), 12977–12989.

Cho, S., Shin, M. H., Kim, Y. K., Seo, J. E., Lee, Y. M., Park, C. H., & Chung, J. H. (2009). Effects of infrared radiation and heat on human skin aging in vivo. *Journal of Investigative Dermatology Symposium Proceedings*, *14*(1), 15–19.

Coblentz, W. W., Stair, R., & Hogue, J. M. (1931). The spectral erythemic reaction of the human skin to ultra-violet radiation. *Proceedings of the National Academy of Sciences*, *17*(6), 401–405.

da Silva Oliveira, C. I., Martinez-Martinez, D., Al-Rjoub, A., Rebouta, L., Menezes, R., & Cunha, L. (2018). Development of a statistical method to help evaluating the transparency/opacity of decorative thin films. *Applied Surface Science*, *438*, 51–58.

Deng, B., Wei, Q., & Gao, W. (2008). Physical properties of Al-doped ZnO films deposited on nonwoven substrates by radio frequence magnetron sputtering. *Journal of Coatings Technology and Research*, *5*(3), 393–397.

Du, Q. G., Alagappan, G., Dai, H., Demir, H. V., Yu, H. Y., Sun, X. W., & Kam, C. H. (2012). UV-blocking ZnO nanostructure anti-reflective coatings. *Optics Communications*, *285*(13–14), 3238–3241.

Du, W., Cai, S., Zhang, Y., & Chen, H. (2021). Preparation and optical application of SiO2-TiO2 composite hardening coatings with controllable refractive index by synchronous polymerization. *Coatings*, *11*(2), 129.

Dyer, J. (2011). Infrared functional textiles. *Functional Textiles for Improved Performance, Protection and Health,* 184–197.

Emami, M., & Goodarzi, R. (2018). Optoelectronic correlations for gold thin films in different annealing temperature. *Optik*, *171*, 397–403.

Erokhin, V., & Fontana, M. P. (2011). Thin film electrochemical memristive systems for bio-inspired computation. In *Journal of Computational and Theoretical*

Nanoscience, 8(3), 313–330.

Fasina, O., Tyler, B., Pickard, M., Zheng, G. H., & Wang, N. (2001). Effect of infrared heating on the properties of legume seeds. *International Journal of Food Science and Technology*, *36*(1), 79–90.

Fernández, E., Fajarí, L., Rodríguez, G., Cócera, M., Moner, V., Barbosa-Barros, L., Kamma-Lorger, C. S., De La Maza, A., & López, O. (2016). Reducing the harmful effects of infrared radiation on the skin using bicosomes incorporating β-carotene. *Skin Pharmacology and Physiology*, *29*(4), 169–177.

Fukuda, K., & Someya, T. (2017). Recent progress in the development of printed thin-film transistors and circuits with high-resolution printing technology. *Advanced Materials, 29*(25), 1602736.

Ge, C., & Zhai, W. (2018). Cellular thermoplastic polyurethane thin film: preparation, elasticity, and thermal insulation performance. *Industrial and Engineering Chemistry Research*, *57*(13), 4688–4696.

Giroire, B., Ali Ahmad, M., Aubert, G., Teule-Gay, L., Michau, D., Watkins, J. J., Aymonier, C., & Poulon-Quintin, A. (2017). A comparative study of copper thin films deposited using magnetron sputtering and supercritical fluid deposition techniques. *Thin Solid Films*, *643*, 53–59.

Goossens, T., & Van Hoof, C. (2020). Thin-film interference filters illuminated by tilted apertures. *Applied Optics*, *59*(5), A112.

Grove, W. R. (1852). VII. On the electro-chemical polarity of gases. *Philosophical Transactions of the Royal Society of London*, *142*, 87–101.

Guo, W. P., Mishra, R., Cheng, C. W., Wu, B. H., Chen, L. J., Lin, M. T., & Gwo, S. (2019). Titanium nitride epitaxial films as a plasmonic material platform:

Alternative to gold. *ACS Photonics*, *6*(8), 1848–1854.

Güzel, E. & Özlüoymak, B., (2015). Elektromanyetik spektrumun tarım makinaları araştırmalarında kullanımı. *Tarım Makinaları Bilimi Dergisi*, *11*(4), 315–320.

Hamed, M. S. G., & Mola, G. T. (2020). Highly stable thin film organic solar cells using poly crystallized silver doped LaPO4. *Solar Energy*, *207*, 157–164.

Harris, S. J., Krauss, G. G., Simko, S. J., Baird, R. J., Gebremariam, S. A., & Doll, G. (2002). Abrasion and chemical-mechanical polishing between steel and a sputtered boron carbide coating. *Wear*, *252*(1–2), 161–169.

Honda, K., & Inoué, S. (1988). Sleep-enhancing effects of far-infrared radiation in rats. *International Journal of Biometeorology*, *32*(2), 92–94.

Houng, B., & Chen, H. Bin. (2012). Investigation of AlF3 doped ZnO thin films prepared by RF magnetron sputtering. *Ceramics International*, *38*(1), 801–809.

Hu, L., Geng, X., Singh, S., Shi, J., Hu, Y., Li, S., Guan, X., He, T., Li, X., Cheng, Z., Patterson, R., Huang, S., & Wu, T. (2019). Synergistic effect of electron transport layer and colloidal quantum dot solid enable PbSe quantum dot solar cell achieving over 10 % efficiency. *Nano Energy*, *64*, 103922.

Hwang, S., Lee, D. H., Lee, I. K., Park, Y. M., & Jo, I. (2014). Far-infrared radiation inhibits proliferation, migration, and angiogenesis of human umbilical vein endothelial cells by suppressing secretory clusterin levels. *Cancer Letters*, *346*(1), 74–83.

Ignatov, I. (2014). Infrared Thermal field emitted from human body. *Journal of Medicine, Physiology and Biophysics*, *1*, 1–12.

Ishizuka, S., Maruyama, T., & Akimoto, K. (2000). Thin-film deposition of Cu2O by reactive radio-frequency magnetron sputtering. *Japanese Journal of Applied Physics, Part 2: Letters*, *39*(8 A), L786.

Jiang, S., Miao, D., Xu, J., Shang, S., Ning, X., & Zhu, P. (2017). Preparation and characterization of shielding textiles to prevent infrared penetration with Ag thin films. *Journal of Materials Science: Materials in Electronics*, *28*(4), 3542–3547.

Jiang, S. X., Qin, W. F., Tao, X. M., Zhang, Z. M., Yuen, C. W. M., Xiong, J., Kan, C. W., Zhang, L., Guo, R. H., & Shang, S. M. (2011). Surface characterization of sputter silver-coated polyester fiber. *Fibers and Polymers*, *12*(5), 616–619.

Jiang, S., Xu, J., Miao, D., Peng, L., Shang, S., & Zhu, P. (2017). Water-repellency, ultraviolet protection and infrared emissivity properties of AZO film on polyester fabric. *Ceramics International*, *43*(2), 2424–2430.

Kaufman, H. R., & Robinson, R. S. (1982). Ion source design for industrial applications. *AIAA Journal*, *20*(6), 745–760.

Kawazoe, H., Yasukawa, M., Hyodo, H., Kurita, M., Yanagi, H., & Hosono, H. (1997). P-type electrical conduction in transparent thin films of CuAlO2. *Nature*, *389*(6654), 939–942.

Keane, J. T., Elangovan, H., Stokes, R. A., & Gunton, J. E. (2018). Vitamin D and the liver—correlation or cause? *Nutrients 10*(4), 496.

Khamseh, S., Alibakhshi, E., Ramezanzadeh, B., & Ganjaee Sari, M. (2021). A tailored pulsed substrate bias voltage deposited (a-C: Nb) thin-film coating on GTD-450 stainless steel: Enhancing mechanical and corrosion protection characteristics. *Chemical Engineering Journal*, *404*, 126490.

Khan, K., Tareen, A. K., Aslam, M., Wang, R., Zhang, Y., Mahmood, A., Ouyang, Z., Zhang, H., & Guo, Z. (2020). Recent developments in emerging two-dimensional materials and their applications. *Journal of Materials Chemistry C*, *8*(2), 387–440.

Khan, M. Z., Baheti, V., Ashraf, M., Hussain, T., Ali, A., Javid, A., & Rehman, A. (2018). Development of Uv protective, superhydrophobic and antibacterial textiles using ZnO and TiO2 nanoparticles. *Fibers and Polymers*, *19*(8), 1647–1654.

Kim, D. G., Han, K. Il, Choi, J. H., & Kim, T. K. (2016). Experimental verification of active IR stealth technology by controlling the surface temperature using a thermoelectric element. *Journal of Mechanical Science and Technology*, *30*(10), 4801–4806.

Kocić, A., Bizjak, M., Popović, D., Poparić, G. B., & Stanković, S. B. (2019). UV protection afforded by textile fabrics made of natural and regenerated cellulose fibres. *Journal of Cleaner Production*, *228*, 1229–1237.

Kumarakuru, H., Cherns, D., & Collins, A. M. (2014). The growth and conductivity of nanostructured ZnO films grown on Al-doped ZnO precursor layers by pulsed laser deposition. *Ceramics International*, *40*(6), 8389–8395.

Lackner, J. M., & Waldhauser, W. (2010). Inorganic PVD and CVD coatings in medicine - A review of protein and cell adhesion on coated surfaces. *Journal of Adhesion Science and Technology*, *24*(5), 925–961.

Lauwerens, W., De Boeck, A., Thijs, M., Claessens, S., Van Stappen, M., & Steenackers, P. (2001). PVD Al-Ti and Al-Mn coatings for high temperature corrosion protection of sheet steel. *Surface and Coatings Technology*, *146–147*, 27–32.

Lee, J., Kim, S., Lee, J., Yang, D., Park, B. C., Ryu, S., & Park, I. (2014). A stretchable strain sensor based on a metal nanoparticle thin film for human motion detection. *Nanoscale*, *6*(20), 11932–11939.

Li, X., Niitsoo, O., & Couzis, A. (2016). Electrostatically assisted fabrication of silver-dielectric core/shell nanoparticles thin film capacitor with uniform metal nanoparticle distribution and controlled spacing. *Journal of Colloid and Interface Science*, *465*, 333–341.

Lin, C. C., Yang, W. C., Chen, M. C., Liu, W. S., Yang, C. Y., & Lee, P. C. (2013). Effect of far infrared therapy on arteriovenous fistula maturation: An open-label randomized controlled trial. *American Journal of Kidney Diseases*, *62*(2), 304–311.

Lin, W. M. M., Yazdani, N., Yarema, O., Volk, S., Yarema, M., Kirchartz, T., & Wood, V. (2019). Simulating nanocrystal-based solar cells: A lead sulfide case study. *Journal of Chemical Physics*, *151*(24), 241104.

Lindner, M. (2020). Effect of substrate strain, aluminum thickness and corona pretreatment on the electrical resistance of physical vapor deposited aluminum coatings. *Coatings*, *10*(12), 1–16.

Liu, B., Guo, J., Hao, R., Wang, L., Gu, K., Sun, S., & Aierken, A. (2020). Effect of Na doping on the performance and the band alignment of CZTS/CdS thin film solar cell. *Solar Energy*, *201*, 219–226.

Liu, Y., Tang, J., Wang, R., Lu, H., Li, L., Kong, Y., Qi, K., & Xin, J. H. (2007). Artificial lotus leaf structures from assembling carbon nanotubes and their applications in hydrophobic textiles. *Journal of Materials Chemistry*, *17*(11), 1071–1078.

Lou, C. W., & Lin, J. H. (2011). Evaluation of bamboo charcoal/stainless steel/TPU composite woven fabrics. *Fibers and Polymers*, *12*(4), 514–520.

Mackie, R. M. (2000). Effects of ultraviolet radiation on human health. *Radiation Protection Dosimetry*, *91*(1–3), 15–18.

Matts, P. J. (2006). Solar ultraviolet radiation: Definitions and terminology. *Dermatologic Clinics*, *24*(1), 1–8.

Maurya, D. K., Sardarinejad, A., & Alameh, K. (2014). Recent developments in R.F. magnetron sputtered thin films for pH sensing applications-an overview. *Coatings 4*(4), 756–771.

Mavrić, Z., Tomšič, B., & Simončič, B. (2018). Recent advances in the ultraviolet protection finishing of textiles. *Tekstilec*, *61*(3), 201–220.

Miao, D. G., Jiang, S. X., Shang, S. M., Chen, Z. M., & Liu, J. (2014). Infrared reflective property of AZO films prepared by RF magnetron sputtering. *Materials Technology*, *29*(6), 321–325.

Miao, D., Hu, H., Li, A., Jiang, S., & Shang, S. (2015). Fabrication of porous and amorphous TiO2 thin films on flexible textile substrates. *Ceramics International*, *41*(7), 9177–9182.

Miao, D., Jiang, S., Liu, J., Ning, X., Shang, S., & Xu, J. (2017). Fabrication of copper and titanium coated textiles for sunlight management. *Journal of Materials Science: Materials in Electronics*, *28*(13), 9852–9858.

Miao, D., Jiang, S., Shang, S., & Chen, Z. (2014). Infrared reflective properties of AZO/Ag/AZO trilayers prepared by RF magnetron sputtering. *Ceramics International*, *40*(8 PART B), 12847–12853.

Miao, D., Jiang, S., Zhao, H., Shang, S., & Zhu, P. (2014). Fabrication of high infrared reflective AZO/Ag/AZO films on polyester fabrics. *Journal of Materials Science: Materials in Electronics*, *26*(2), 1198–1204.

Miao, D., Zhao, H., Peng, Q., Shang, S., & Jiang, S. (2015). Fabrication of high infrared reflective ceramic films on polyester fabrics by RF magnetron sputtering.

Ceramics International, *41*(1), 1595–1601.

Mohammad Bagher, A. (2015). Types of solar cells and application. *American Journal of Optics and Photonics*, *3*(5), 94.

Nelis, T., & Pallosi, J. (2006). Glow discharge as a tool for surface and interface analysis. In *Applied Spectroscopy Reviews 41*(3), 227–258.

Nomura, K., Ohta, H., Takagi, A., Kamiya, T., Hirano, M., & Hosono, H. (2004). Room-temperature fabrication of transparent flexible thin-film transistors using amorphous oxide semiconductors. *Nature*, *432*(7016), 488–492.

Okuhara, Y., Kato, T., Matsubara, H., Isu, N., & Takata, M. (2011). Near-infrared reflection from periodically aluminium-doped zinc oxide thin films. *Thin Solid Films*, *519*(7), 2280–2286.

Pandel, R., Poljšak, B., Godic, A., & Dahmane, R. (2013). Skin photoaging and the role of antioxidants in its prevention. *ISRN Dermatology*, *2013*, 1–11.

Park, C., Seo, S., Shin, H., Sarwade, B. D., Na, J., & Kim, E. (2015). Switchable silver mirrors with long memory effects. *Chemical Science*, *6*(1), 596–602.

Patil, S. A., Hussain, S., Shrestha, N. K., Mengal, N., Jalalah, M., Jung, J., Park, J. G., Choi, H., Kim, H. S., & Noh, Y. Y. (2020). Facile synthesis of cobalt–nickel sulfide thin film as a promising counter electrode for triiodide reduction in dye-sensitized solar cells. *Energy*, *202*, 117730.

Pejova, B., & Grozdanov, I. (2006). Structural and optical properties of chemically deposited thin films of quantum-sized bismuth(III) sulfide. *Materials Chemistry and Physics*, *99*(1), 39–49.

Rossnagel, S. M. (1998). Directional and ionized physical vapor deposition for microelectronics applications. *Journal of Vacuum Science & Technology B: Microelectronics and Nanometer Structures*, *16*(5), 2585.

Rossnagel, S. M. (2003). Thin film deposition with physical vapor deposition and related technologies. *Journal of Vacuum Science & Technology A: Vacuum, Surfaces, and Films*, *21*(5), S74–S87.

Şahan, M., Tokat, Ö., & Okur, Y. (2015). Osmaniye ' de günlük toplam güneş ışınım ölçümleri. *SDU Journal of Science (E-Journal)*, *10*(2), 97–105.

Saraf, L. V., Patil, S. I., Ogale, S. B., Sainkar, S. R., & Kshirsager, S. T. (1998). Synthesis of nanophase TiO2 by ion beam sputtering and cold condensation technique. *International Journal of Modern Physics B*, *12*(25), 2635–2647.

Sarma, S. (2021). Dependence of resistivity on thickness of vacuum deposited copper thin films. *Advanced Science, Engineering and Medicine*, *12*(8), 1125–1129.

Savale, P. A. (2016). Physical vapor deposition (PVD) methods for synthesis of thin films: A comparative study. *Scholars Research Library Archives of Applied Science Research*, *8*(5), 1-8.

Shi, Q., Zhou, K., Dai, M., Hou, H., Lin, S., Wei, C., & Hu, F. (2013). Room temperature preparation of high performance AZO films by MF sputtering. *Ceramics International*, *39*(2), 1135–1141.

Shi, W., Gao, B., Tu, G., Li, S., Hao, Y., & Yu, F. (2010). Effect of neodymium on primary silicon and mechanical properties of hypereutectic Al-15Si alloy. *Journal of Rare Earths*, *28*(SUPPL. 1), 367–370.

Simon, R. W., Platt, C. E., Lee, A. E., Lee, G. S., Daly, K. P., Wire, M. S., Luine, J. A., & Urbanik, M. (1988). Low-loss substrate for epitaxial growth of high-temperature superconductor thin films. *Applied Physics Letters*, *53*(26), 2677–

2679.

Smecca, E., Maita, F., Pellegrino, G., Vinciguerra, V., La Magna, L., Mirabella, S., Maiolo, L., Fortunato, G., Condorelli, G. G., & Alberti, A. (2015). AlN texturing and piezoelectricity on flexible substrates for sensor applications. *Applied Physics Letters*, *106*(23), 232903.

Sönmezoğlu, S., Koç, M., & Akin, S. (2012). İnce film üretim teknikleri. In *Erciyes Üniversitesi Fen Bilimleri Enstitüsü Fen Bilimleri Dergisi 28*(5), 389-404.

Syms, R. R. A., Solymar, L., Young, I. R., & Floume, T. (2010). Thin-film magneto-inductive cables. *Journal of Physics D: Applied Physics*, *43*(5), 055102.

Taglauer, E. (1990). Surface cleaning using sputtering. *Applied Physics A Solids and Surfaces*, *51*(3), 238–251.

Thai, N. X., Van Duy, N., Van Toan, N., Hung, C. M., Van Hieu, N., & Hoa, N. D. (2020). Effective monitoring and classification of hydrogen and ammonia gases with a bilayer Pt/SnO2 thin film sensor. *International Journal of Hydrogen Energy*, *45*(3), 2418–2428.

Tverjanovich, A., Khomenko, M., Bereznev, S., Fontanari, D., Sokolov, A., Usuki, T., Ohara, K., Le Coq, D., Masselin, P., & Bychkov, E. (2020). Glassy GaS: Transparent and unusually rigid thin films for visible to mid-IR memory applications. *Physical Chemistry Chemical Physics*, *22*(44), 25560–25573.

Ulbrich, C., Gerber, A., Hermans, K., Lambertz, A., & Rau, U. (2013). Analysis of short circuit current gains by an anti-reflective textured cover on silicon thin film solar cells. *Progress in Photovoltaics: Research and Applications*, *21*(8), 1672–1681.

Wei, Q., Xu, Q., Cai, Y., & Wang, Y. (2008). Evaluation of the interfacial bonding between fibrous substrate and sputter coated copper. *Surface and Coatings Technology*, *202*(19), 4673–4680.

Wei, R., Vajo, J. J., Matossian, J. N., & Gardos, M. N. (2002). Aspects of plasma-enhanced magnetron-sputtered deposition of hard coatings on cutting tools. *Surface and Coatings Technology*, *158–159*, 465–472.

Xu, Y. J., Liao, J. X., Cai, Q. W., & Yang, X. X. (2013). Preparation of a highly-reflective TiO2/SiO2/Ag thin film with self-cleaning properties by magnetron sputtering for solar front reflectors. *Solar Energy Materials and Solar Cells*, *113*, 7–12.

Yip, J., Jiang, S., & Wong, C. (2009). Characterization of metallic textiles deposited by magnetron sputtering and traditional metallic treatments. *Surface and Coatings Technology*, *204*(3), 380–385.

Yoo, S. M., Yoon, S. J., Anta, J. A., Lee, H. J., Boix, P. P., & Mora-Seró, I. (2019). An equivalent circuit for perovskite solar cell bridging sensitized to thin film architectures. *Joule*, *3*(10), 2535–2549.

Yuce, I. (2017). Uzak kizilötesi işin yayan kumaş ve iplikler. *Trakya University Journal of Engineering Sciences*, *18*(2), 145–151.

Zambrano, D. F., Villarroel, R., Espinoza-González, R., Carvajal, N., Rosenkranz, A., Montaño-Figueroa, A. G., Arellano-Jiménez, M. J., Quevedo-Lopez, M., Valenzuela, P., & Gacitúa, W. (2021). Mechanical and microstructural properties of broadband anti-reflective TiO2/SiO2 coatings for photovoltaic applications fabricated by magnetron sputtering. *Solar Energy Materials and Solar Cells*, *220*, 110841.

Zhao, Z., Tay, B. K., & Yu, G. (2004). Room-temperature deposition of amorphous titanium dioxide thin film with high refractive index by a filtered cathodic vacuum arc technique. *Applied Optics*, *43*(6), 1281–1285.